Available online at www.sciencedirect.com
ScienceDirect
Journal of Power Sources 160 (2006) 872–891
JOURNAL OF POWER SOURCES
www.elsevier.com/locate/jpowsour

Review

High temperature PEM fuel cells

Jianlu Zhang [a], Zhong Xie [a], Jiujun Zhang [a,*], Yanghua Tang [a], Chaojie Song [a], Titichai Navessin [a], Zhiqing Shi [a], Datong Song [a], Haijiang Wang [a], David P. Wilkinson [a,b], Zhong-Sheng Liu [a], Steven Holdcroft [a,c,**]

[a] *Institute for Fuel Cell Innovation, National Research Council Canada, Vancouver, BC, Canada V6T 1W5*
[b] *Department of Chemical and Biological Engineering, University of British Columbia, Vancouver, BC, Canada V6T 1Z4*
[c] *Department of Chemistry, Simon Fraser University, Burnaby, BC, Canada V5A 1S6*

Received 18 April 2006; received in revised form 12 May 2006; accepted 16 May 2006
Available online 30 June 2006

Abstract

There are several compelling technological and commercial reasons for operating H_2/air PEM fuel cells at temperatures above 100 °C. Rates of electrochemical kinetics are enhanced, water management and cooling is simplified, useful waste heat can be recovered, and lower quality reformed hydrogen may be used as the fuel. This review paper provides a concise review of high temperature PEM fuel cells (HT-PEMFCs) from the perspective of HT-specific materials, designs, and testing/diagnostics. The review describes the motivation for HT-PEMFC development, the technology gaps, and recent advances.

HT-membrane development accounts for ~90% of the published research in the field of HT-PEMFCs. Despite this, the status of membrane development for high temperature/low humidity operation is less than satisfactory. A weakness in the development of HT-PEMFC technology is the deficiency in HT-specific fuel cell architectures, test station designs, and testing protocols, and an understanding of the underlying fundamental principles behind these areas. The development of HT-specific PEMFC designs is of key importance that may help mitigate issues of membrane dehydration and MEA degradation.

Keywords: High temperature; PEMFCs; Development; Testing and diagnostics

Contents

* Corresponding author. Tel.: +1 604 221 3087; fax: +1 604 221 3001.
** Corresponding author. Tel.: +1 604 291 3765.
E-mail addresses: jiujun.zhang@nrc.gc.ca (J. Zhang), holdcrof@sfu.ca (S. Holdcroft).

0378-7753/$ – see front matter © 2006 Elsevier B.V. All rights reserved.
doi:10.1016/j.jpowsour.2006.05.034

1. Introduction

H_2/air fuel cells based on proton-exchange membranes have many attractive features, including high power density, rapid start-up, high efficiency, which makes them a promising clean energy technology. Great advances have been made in PEM fuel cell development. Catalyst loading has been significantly reduced, power density has been increased, and prototype PEM fuel cell vehicles have been successfully tested on many continents. In spite of these successes, there is strong need to enhance the performance of current PEM fuel cells. Several technical obstacles hinder their widespread commercialization for transportation and stationary application sectors. These include inadequate water and heat management, the intolerance to impurities such as CO, sluggish electrochemical cathode kinetics, and their high cost.

Recent progress in H_2/air PEM fuel cells has focused on the need to develop PEM fuel cells that operate above 100 °C. There are several compelling reasons for operating at a higher temperature [1]: (i) Electrochemical kinetics for both electrode reactions are enhanced; (ii) water management can be simplified because only a single phase of water need to be considered; (iii) the cooling system is simplified due to the increased temperature gradient between the fuel cell stack and the coolant; (iv) waste heat can be recovered as a practical energy source; (v) CO tolerance is dramatically increased thereby allowing fuel cells to use lower quality reformed hydrogen.

Research advances of high temperature PEM fuel cells (HT-PEMFCs) are occurring at a rapid pace and on many disciplinary fronts. This review aims to provide a concise, but broad review of the field of HT-PEMFCs from the perspective of materials requirements and characterization. Part I of this review provides background theory that supports and motivates HT-PEMFC development. Part II describes the major technology gaps that must be addressed for their commercialization and widespread use. Part III addresses recent advances in functional materials and component design, and requirements for the testing and diagnosis of emerging materials and components.

2. Part I: advantages of high temperature operation

2.1. Improved cathode kinetics

The exchange current density for the electrochemical oxygen reduction reaction (ORR, $\sim 10^{-8}$ to 10^{-9} A cm^{-2}) is much smaller than that of the hydrogen oxidation reaction (HOR, $\sim 10^{-3}$ to 10^{-4} A cm^{-2}). Since HOR at the Pt nanoparticle/PEM interface is reversible [2], the overpotential for HOR is negligibly small compared with that of ORR when the anode is adequately hydrated. The overall electrochemical kinetics of PEMFCs is therefore determined by the relatively slow oxygen reduction reaction (ORR). However, at operating temperatures above 100 °C, anode dehydration may become a significant challenge.

The performance of a PEMFC in the kinetically controlled regime can be represented by the Tafel equation:

$$E = E_{\text{rev}} + b \log i_0 - b \log i \tag{1}$$

$$b = -2.3\frac{RT}{\alpha n F} \tag{2}$$

where E, E_{rev}, b, i, i_0, n and α are the electrode potential, reversible potential, Tafel slope, current density, exchange current density, the number of electrons transferred in the rate determining step and the transfer coefficient, respectively. The variation of E_{rev}, i_0 and b with temperature are discussed below:

2.1.1. Effect of temperature on E_{rev} and OCV

E_{rev} is related to temperature according to Eq. (5), which is derived from Eqs. (3) and (4):

$$\left(\frac{\partial E_{\text{rev}}}{\partial T}\right)_{\text{P}} = \frac{E_{\text{rev}} - E^0_{\text{rev}}}{T - 298} \tag{3}$$

$$\left(\frac{\partial E_{\text{rev}}}{\partial T}\right)_{\text{P}} = \left(\frac{\Delta S}{nF}\right)_{\text{P}} \tag{4}$$

$$E_{\text{rev}} = E^0_{\text{rev}} + \left(\frac{\partial E_{\text{rev}}}{\partial T}\right)_{\text{P}} (T - 298)$$

$$= E^0_{\text{rev}} + \left(\frac{\Delta S}{nF}\right)_{\text{P}} (T - 298) \tag{5}$$

ΔS for the H_2/O_2 reaction is negative below 100 °C, because gases are converted to liquid, thus, E_{rev} decreases with increasing temperature. This effect is less pronounced above 100 °C when gaseous reactants are converted to gaseous product. Below 100 °C the change in entropy (ΔS°) for the H_2/O_2 reaction is ca. $-163.5\,\text{J K}^{-1}\,\text{mol}^{-1}$, while above 100 °C, ΔS° is approximately $-44.5\,\text{J K}^{-1}\,\text{mol}^{-1}$. These values, corresponding to $\partial E_{\text{rev}}/\partial T$ or $\Delta S/nF$ in Eq. (5), are $-0.85\,\text{mV K}^{-1}$ (<100 °C) and $-0.23\,\text{mV K}^{-1}$ (>100 °C).

For the electrochemical reaction shown in Eq. (6), the thermodynamic OCV (open-circuit voltage) can be described by Eq. (7). Consequently, the thermodynamic OCV decreases with increasing temperature, especially above 100 °C, due to the increase of P_{H_2O}:

$$O_2 + 2H_2 \Leftrightarrow 2H_2O \tag{6}$$

$$\text{OCV} = E^0_{\text{rev}} + \left(\frac{\Delta S}{nF}\right)_{\text{P}} (T - 298) + \frac{RT}{2F} \ln \frac{P_{H_2} P_{O_2}^{1/2}}{P_{H_2O}} \tag{7}$$

The temperature-dependent thermodynamic open-circuit voltage for the overall reaction (6) can be estimated using the relation (Eq. (8)) [3–5]:

$$\text{OCV} = 1.23 - 0.9 \times 10^{-3}(T - 298)$$

$$+2.3\frac{RT}{4F} \log \frac{P^2_{H_2} P_{O_2}}{P^2_{H_2O}} \tag{8}$$

Xu et al. [6] calculated the theoretical OCV using the following equation:

$$\text{OCV} = 1.482 - 0.000845T + RT \ln \frac{P_{H_2} P_{O_2}^{0.5}}{P_{H_2O}} \tag{9}$$

They observed that increasing the fuel cell temperature from 60 to 120 °C, while maintaining a constant relative humidity (RH), caused the theoretical OCV to decrease from 1.22 to 1.14 V due to the increase in water partial pressure—in accordance with theory.

2.1.2. Effect of temperature on the Tafel slope

For both the HOR and ORR, the dependence of b on temperature can be derived by differentiating Eq. (2):

$$\frac{\partial b}{\partial T} = -\frac{2.3R}{\alpha n F} \tag{10}$$

Assuming that the reaction mechanism and α is independent of temperature, b varies linearly with temperature. For $\alpha n = 1$, $\partial b/\partial T \approx 0.2\,\text{mV K}^{-1}$. However, several groups [7–11] report two sets of Tafel slopes that are differentiated by the current density regime. One Tafel parameter corresponds to oxygen reduction at a Pt oxide-covered surface (Temkin adsorption conditions, low current density, $b = 60$ mV/decade); and the other, at a Pt oxide-free surface (Langmuirian conditions, high current density and $b = 120$ mV/decade). Thus, the $\sim 0.2\,\text{mV K}^{-1}$ increase predicted for a temperature increase above 100 °C may be masked by changes in the reaction mechanism of ORR from Temkin conditions [10,11] and the corresponding change in Tafel slope and increase in exchange current density with increasing temperature. Experimentally, the Tafel slope corresponding to the ORR was found to increase with temperature in the low current density region, while it was independent of temperature in the high current density region [9].

2.1.3. Effect of temperature on i_0

Kinetic parameters associated with the ORR at Pt/PEM interfaces have been investigated using EIS (electrochemical impedance spectroscopy) and LSV (linear sweep voltammetry) in a solid-state electrochemical cell using microelectrodes [12]. It is found that i_0 increases with temperature. Beattie et al. [13] report i_0 values for Nafion® 117 and BAM® 407, an experimental sulfonated polytrifluorostyrene-based membrane, ranging from 2.08×10^{-10} to $3.71 \times 10^{-9}\,\text{A cm}^{-2}$ and 8.80×10^{-11} to $4.38 \times 10^{-10}\,\text{A cm}^{-2}$, respectively, over the temperature range 303–343 K. Parthasarathy et al. [9] report that i_0 at Pt/Nafion® 117 interfaces in the low current density region increases from 1.69×10^{-10} to $5.54 \times 10^{-9}\,\text{A cm}^{-2}$ as the temperature is increased from 303 to 343 K. It is likely that the increase in i_0 will deviate from this relationship above 100 °C but data at temperatures >100 °C are notably absent from the literature, presumably due to the experimental difficulties in operating solid state cells at elevated temperature and lower humidity.

2.2. Improved tolerance of the catalyst to contaminants

The vast majority of reported data on the performance of H_2/air fuel cells are obtained using pure hydrogen as fuel but from the technological point of view this is unrealistic because high purity hydrogen may not be readily available. It may be preferential to use hydrogen-rich gases as fuel. On-site generation of hydrogen prepared using reforming reactions, such as the water–gas shift reaction, preferential oxidation, membrane separation or methanol oxidation, from various organic fuels (e.g., methanol, natural gas, gasoline, etc.) are attractive alternatives to "stored" hydrogen. However, reformate gases generally contain traces of carbon monoxide (CO) which strongly adsorb on the surface of Pt, occupying hydrogen oxidation reaction (HOR) sites, as illustrated in Fig. 1. Trace CO dramatically reduces the activity of Pt or Pt-alloys in the anode.

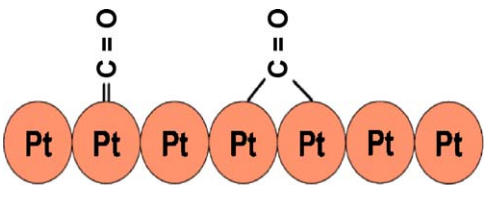

Fig. 1. Adsorption of CO on Pt.

It is reported that at 80 °C, CO concentrations as low as 10–20 ppm causes a significant loss in cell performance [14]. As a consequence, purification of the reformate gas is necessary in order to reduce CO concentrations to <10 ppm. Qi et al. [15] report that trace amounts of CO also poison the cathode after passing through the membrane. Considerable effort has been made to reduce the effect of CO. These include (1) feeding oxidant (O_2 or H_2O_2) into the fuel; (2) advanced purification of reformate gas; (3) developing CO-tolerant electrocatalysts (e.g., PtRu/C, PtSn/C). However, all approaches to-date have significant drawbacks and/or performance issues. For instance, the addition of oxidant to the fuel stream decreases fuel utilization and compromises safety; additional fuel processing increases system complexity and cost; and the effectiveness of new CO-tolerant electrocatalysts is far from satisfactory. An alternative is to increase the operating temperature of the PEMFC to effectively alleviate CO adsorption on the catalyst.

It is well known that adsorption of CO on Pt is associated with a high negative entropy, indicating that adsorption is strongly favoured at low temperatures, and disfavoured at higher temperatures [16–19]. At 130 °C, for example, Pt-based catalysts can tolerate up to 1000 ppm CO [20]. A thermodynamic analysis of the temperature requirements for CO tolerance was conducted by Yang et al. [21]. They report that increased tolerance to CO is related to the thermodynamics of adsorption of CO and H_2 on Pt. Adsorption is Langmuirian in nature. CO adsorbs associatively on Pt below 500 K, whereas H_2 adsorbs dissociatively:

$$CO(g) + Pt \rightarrow Pt\text{–}CO \quad (11)$$

$$H_2 + 2Pt \rightarrow 2Pt\text{–}H \quad (12)$$

The fractional coverages (θ) of CO and H_2 on the surface of the catalyst are given by Eqs. (13) and (14):

$$\theta_{CO} = \frac{K_{CO} P_{CO}}{1 + K_{CO} P_{CO} + K_H^{1/2} P_{H_2}^{1/2}} \quad (13)$$

$$\theta_H = \frac{K_H^{1/2} P_{H_2}^{1/2}}{1 + K_{CO} P_{CO} + K_H^{1/2} P_{H_2}^{1/2}} \quad (14)$$

where K_{CO} and K_H are the equilibrium constants for adsorption, and P_{CO} and P_{H_2} are the partial pressures of CO and H_2 in the gas phase, respectively. Because hydrogen adsorption is less exothermic than CO and H_2 adsorption requires two adsorption sites, increasing the temperature leads to a beneficial shift towards higher H_2 coverage at the expense of CO coverage.

In Fig. 2, a plot is shown illustrating the equilibrium coverage of CO on Pt at CO concentrations ranging from 1 to 100 ppm with a H_2 pressure of 0.5 bar. The enthalpies of adsorption are those determined on a Pt (1 1 1) surface, and the adsorption entropies are determined from desorption kinetics as described by Benziger [22]. It is clear that operation at higher temperatures increases the ability of the fuel cell anode to perform in the presence of small amounts of CO by decreasing the coverage of CO on the catalyst surface. Similar adsorption curves are also reported by Adjemian et al. [23] and Malhotra et al. [24]. They report that hydrogen coverage increases from 0.02 monolayers at 350 K (77 °C), to 0.39 monolayers at 400 K (127 °C). Since current density is proportional to hydrogen coverage on the anode, an increase in temperature from 80 to 130 °C increases the current density by a factor of 20 [23].

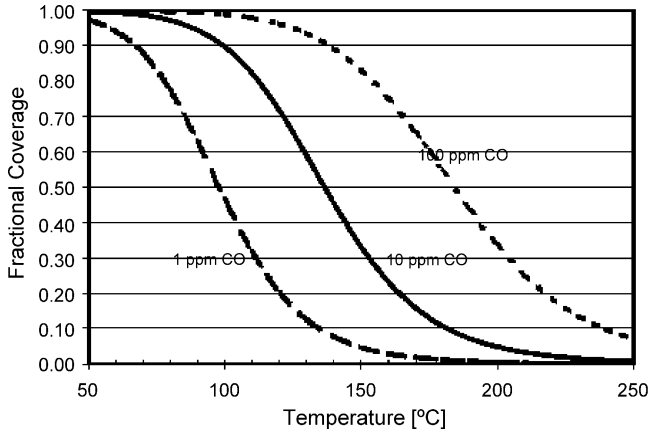

Fig. 2. CO coverage on a platinum as a function of temperature and CO concentration. The partial pressure of H_2 is 0.5 bar [21].

Bellows et al. [25] studied the electrooxidation reaction kinetics of CO in 1 M H_2SO_4 on polycrystalline Pt using linear sweep voltammetry (LSV) and found that the CO electrooxidation rate increases with increasing temperatures. The effects of CO adsorption onto Pt during high temperature operation of a PEMFC (>120 °C) have also been reported [19,24,26]. The study conducted by Lakshmanan et al. [27] using polyetheretherketone membranes indicates that for standard Pt–Ru catalysts an increase in operating temperature from 70 to 120 °C improves the CO tolerance from 50 to 1300 pm. Li et al. [19] investigated the effect of poisoning of carbon supported Pt in PEMFCs over a temperature range 125–200 °C with phosphoric acid-doped polybenzimidazole (PBI) membranes, and found that CO poisoning can be sufficiently suppressed at elevated temperature. As shown in Fig. 3, by defining the CO tolerance as a voltage loss of <10 mV, it is estimated that 3% CO in H_2 can be tolerated for current densities up to 0.8 A cm^{-2} at 200 °C; 0.1% CO can be tolerated for current densities <0.3 A cm^{-2} at 125 °C; whereas only 25 ppm CO can be tolerated at 80 °C for current densities up

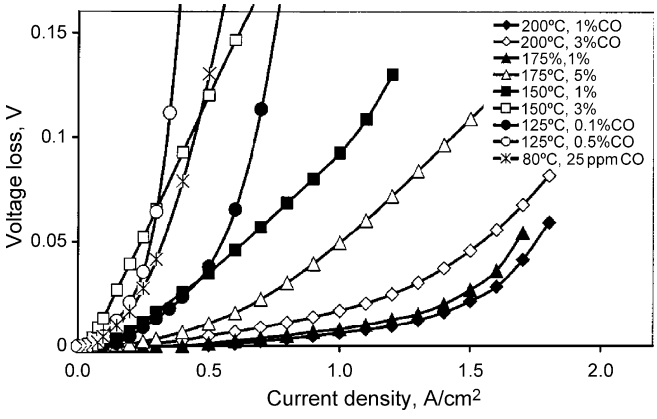

Fig. 3. Loss in voltage as a function of current density at different temperatures and different CO concentrations [19].

to 0.2 A cm^{-2}. CO tolerance is dramatically enhanced, from 10 to 20 ppm at 80 °C to 1000 ppm at 130 °C, and up to 30,000 ppm at 200 °C [19]. This high CO tolerance above 130 °C renders it possible for a fuel cell to use hydrogen directly from a simple reformer.

2.3. Improved water management and gas transport

2.3.1. Water management

Water management in PEM fuel cells requires careful consideration because it affects the overall system power and system efficiency. For a PEM fuel cell operating below 100 °C, a lack of water in the membranes and gas diffusion electrodes decreases their proton conductivity and significantly increases the cell resistance. Excessive water in the cathode causes "flooding", which restricts oxygen transport through the porous gas diffusion electrode. Operating a cell above at 100 °C may mitigate potential problems associate with flooding but they exacerbate issues associated with dehydration. In order to understand this paradox in finer detail, the dominating factors that determine water transport need to be discussed.

Fig. 4 illustrates the different modes of water transport through PEMFCs. The term electro-osmotic drag is characterized by water that is carried by protons as they transverse the membrane from anode to cathode. The production of water at the cathode results in a gradient of water content across the membrane that may result in back diffusion of water from cathode to anode. If a differential pressure exists, hydraulic pressure may also force water from cathode to anode. In the absence of the latter, the net water flux across the membrane is a combination of diffusion and electro-osmotic drag, which has a profound impact on fuel cell performance.

The effect of cathode flooding on FC performance has been simulated using the agglomerate model for the cathode catalyst layer [28]. The detailed parameters used in the simulation are not presented here but were chosen from values typically found in the literature for a cathode operating under room temperature and ambient pressure. For the purpose of illustrating the dependence of cathode performance, values of D_{CL}^{eff} (effective diffusion coefficient of O_2 through the catalyst layer) were varied from 10^{-1} cm^2 s^{-1} (bulk diffusion coefficient in gaseous phase) to 10^{-6} cm^2 s^{-1} (bulk diffusion coefficient in liquid phase). The simulated polarization curves are presented in Fig. 5.

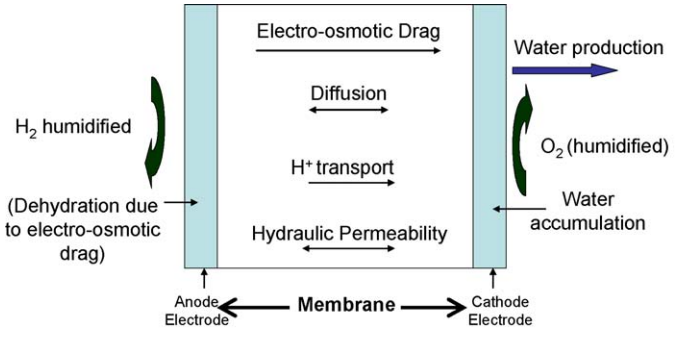

Fig. 4. Schematic drawing illustrating the modes of water transport in an operating H_2/O_2 PEMFC.

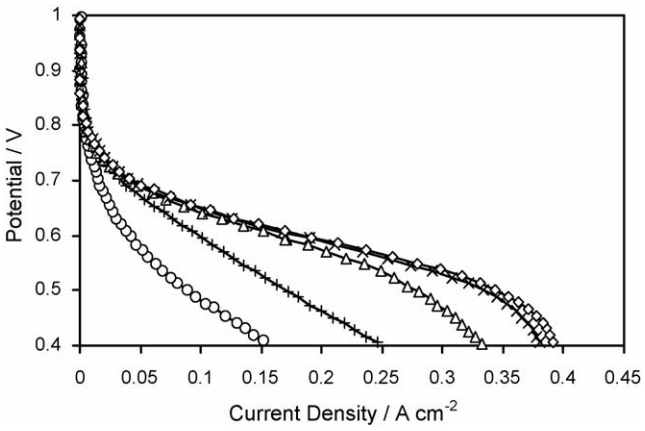

Fig. 5. Dependence of cathode performance on the effective diffusion coefficient in the catalyst layer (D_{CL}^{eff}) [28]; 0.1 cm^2 s^{-1} (—), 10^{-2} cm^2 s^{-1} (◊), 10^{-3} cm^2 s^{-1} (×), 10^{-4} cm^2 s^{-1} (Δ), 10^{-5} cm^2 s^{-1} (+) and 10^{-6} cm^2 s^{-1} (◯).

In the mass transport controlled region the electrode overpotential is sufficiently high that the current density is limited by the rate of reactant supplied to the reactive sites. Since D_{GDL}^{eff} (effective diffusion coefficient of O_2 through the gas diffusion layer) is normally much higher than D_{CL}^{eff}, the mass transport limitation occurs predominantly in the catalyst layer. A decrease in D_{CL}^{eff} reduces the electrode performance at moderate (~0.7 V) and low (~0.4 V) potentials.

The agglomerate model [29–31] and percolation theory [32,33] have been used to analyze fuel cell data of experimental membranes. Fig. 6 shows schematic diagram of water transport in a fuel cell using low and high IEC membranes [34]. Under the fuel cell conditions employed (<100 °C) membranes with higher IEC (ion exchange capacity, defined as the number of chemical equivalents of ion-exchange sites per gram of membrane) were found to exhibit higher gas diffusion rate at the cathodes, were less prone to dehydration of the anode, and consequently showed improved fuel cell performance. These attributes were directly linked to the higher water content in

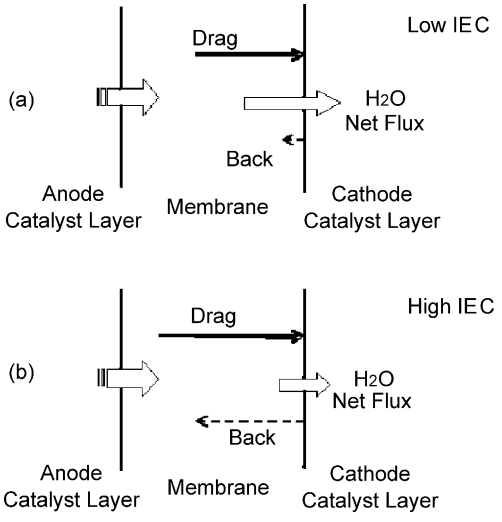

Fig. 6. Schematic diagram illustrating different scenarios of water transport in a fuel cell using (a) low IEC and (b) high IEC membranes. The length of the arrows represent relative extents of water transport [34].

the membranes and the ability to facilitate fuel cell water management by allowing more rapid water transfer from cathode to anode. Thus, membranes that promote water transport are more likely to better mitigate problems of dehydration of the anode. However, high IEC membranes exhibit a higher propensity to dehydrate and usually require extensive humidification. The issue of water transport from cathode to anode is expected to be greatly exacerbated for high temperature membranes operating above 100 °C where liquid water is absent.

2.3.2. Effect of temperature on gas diffusion, solubility, and permeability

Gas diffusion through the solid polymer electrolyte, in both the membrane and the gas diffusion electrode, are important aspects to consider. Generally, gas diffusion coefficients increase with temperature whereas solubility decreases. The relationship between the oxygen diffusion coefficient, $D(O_2)$, in hydrated Nafion membranes as a function of temperature is given by the relationship [4,35]:

$$D_{O_2} = 3.1 \times 10^{-3} \exp\left(-\frac{2768}{T}\right) \quad (15)$$

where T is the temperature (K). The corresponding equation for oxygen solubility was used by Bernardi and Verbrugge [36] to develop the Henry's law expression:

$$K_{O_2} = 1.33 \times 10^{6} \exp\left(-\frac{666}{T}\right) \quad (16)$$

where K_{O_2} is in units of atm cm^3 mol^{-1}. Parthasarathy et al. [9] reported that the diffusion coefficient of O_2 increased from 9.95×10^{-7} to 6.22×10^{-6} while the solubility of O_2 decreased from 9.34×10^{-6} to 4.33×10^{-6} in Nafion 117 for an oxygen pressure of 5 atm. Mitsushima et al. [37] studied the effect of equivalent weight (EW) on these parameters in Nafion® and Aciplex® membranes. Their results indicated that the diffusion coefficients increased with increasing exchange capacity and with increasing temperature, whereas oxygen solubility decreased with increasing temperature and exchange capacity. The dependences of diffusion coefficient on the temperature and the equivalent weight are larger than those of the solubility, thus oxygen permeability, the product of diffusion coefficient and solubility, increases with increasing temperature and ion exchange capacity [38]. Similar conclusions are reported by other researchers [12,39–43].

Data for the diffusion on hydrogen in polymer electrolytes are scarce. Yeo and McBreen [44] obtained the following relation for the diffusivity of dissolved hydrogen in Nafion with temperature:

$$D_{H_2} = 4.1 \times 10^{-3} \exp\left(-\frac{2602}{T}\right) \quad (17)$$

Ota et al. [41] reported that the diffusion coefficient of H_2 increases with increasing temperature, while the solubility of H_2 decreases, i.e., the same trend as observed for O_2. However, the diffusion coefficient of hydrogen is one order higher than that of oxygen, whereas its solubility is lower. Similar to oxygen, the permeability of H_2 increases with temperature.

2.3.3. Vapor water versus liquid water for O_2 mass transport improvement

The diffusion coefficient of oxygen through water vapor is several orders of magnitude larger than through liquid water. With increasing operating temperature (for a given current density), the ratio of liquid water to water vapor inside cathode catalyst layers and gas diffusion layers decreases. This will serve to increase the effective diffusion coefficient of oxygen. Therefore, high temperature operation facilitates oxygen transport through the gas diffusion layers and the cathode catalyst layers and should lead to an increase in fuel cell performance in the mass transport controlled regime.

2.3.4. Simpler flowfield design without the presence of two phase flow in the channel

The main purpose of a flow field is to provide a uniform reactant distribution over the entire electrode surface area. Since the accumulation of liquid water is a common problem in conventional PEMFCs, the flow field is also designed to promote facile removal of water removal. The flow field plate thus includes both a network of passages for supplying fuel and oxidant to the flow field and a network of passages for receiving discharged gases. The flow field can consist of a plurality of flow sectors having separate inlets and outlets communicating with the networks of supply and exhaust flow passages. Because there is proportionally little or no liquid water present in the fuel cell above 100 °C liquid water management will be simplified, and flow fields may be designed without having to consider two-phase flow.

2.4. Other benefits of high temperature operation

About 40–50% of the energy produced by a PEM fuel cell is dissipated as heat [45] due to thermodynamically irreversible reactions, changes in entropy and Joule heating [46]. Distributions of temperature in an operating fuel cell are therefore expected. The effect on cell performance is significant because of their influence on the transport of water/gaseous species, and the inherent rates of electrochemical reactions. Excessive cell temperatures cause membrane and electrode dehydration, shrinkage and cracking; while low temperatures may lead to flooding. Adequate thermal management is therefore a necessity for PEM fuel cells to achieve high performance, efficiency, durability, and reliability.

A PEMFC operating at 80 °C with an efficiency of 40–50% produces a large amount of heat that must be removed in order to maintain that temperature [1]. As rationalized by Frank [47], the cooling systems of modern vehicles based on the internal combustion engine (ICE) reject <40% of the waste heat; exhaust gases remove the large fraction of excess heat. In contrast, a PEMFC stack operating at 80 °C must reject all the heat produced via the cooling system. The heat rejection capability of the fuel cell system operating below 100 °C is very inefficient, requiring elaborate cooling systems and high surface area heat exchangers.

Operating fuel cells above 100 °C allows for easier heat rejection because of the greater temperature difference between the

fuel cell and ambient environment. As result, the cooling system may be simplified, and the mass-specific and volume-specific power density of the fuel cell system thereby increased. A higher temperature waste heat can also be recovered as steam, which in turn can be used either for direct heating, steam reforming, or pressurized operation. If the operational temperature is much higher, e.g., >200 °C, steam can be produced directly from a fuel cell stack, which can be used directly for heating. Under higher temperature operating conditions, the overall system efficiency is significantly increased.

If PEM fuel cells are exposed to environments that allow water inside the cell to freeze, the volume change of water may deform the structure of the catalytic layer leading to a reduction of the specific surface area and Pt utilization and mechanical failures. This will increase activation polarization and contact resistances resulting in a lower cell performance [48]. High temperature fuel cells are expected to contain minimal liquid water. Hence, subjecting the cell to sub-zero temperatures will have less of an impact, thus, improving their stability and durability.

Under low temperature operation conditions, an FC stack is often purged with dry gas after shutdown, in order to prevent it from suffering from the effects of freezing of internal water [49,50]. This creates another layer of complexity and adds to the cost of the complete system. Moreover, although water is eliminated from channels and gas diffusion layers, water may still exist in the membrane and in the pores of catalyst layers [51]. The absence of liquid water in the membranes, catalyst layers, and flow fields of high temperature fuel cells circumvents the need to undertake complex shutdown procedures. The absence of frozen water may also speed up cold start-up of a fuel cell stack.

Finally, in order to understand the stability and reliability of PEM fuel cells, it is necessary to investigate chemical, morphological and mechanical changes that take place within various components during operation. At temperatures below 100 °C these changes may take place very slowly, and cells often require extensive periods of operation in order to elucidate degradation pathways. Operating a fuel cell at elevated temperature (120 or 150 °C) accelerates these degradation pathways so that they may be studied over a shorter timeframe. In this context, HT-PEMFCs may serve as an accelerated test bench for emerging materials, components and fuel cell designs.

3. Part II: challenges of operating PEMFCs at high temperature

Although operating PEMFCs at temperatures above 100 °C has many attractive features, there are several major challenges. For example, lower temperature PEMFCs employ aqueous-based polyelectrolyte membranes, for which the proton conductivity depends strongly upon the relative humidity. At higher operating temperature, membrane dehydration and the subsequent decrease in proton conductivity is a significant issue. In addition, various components of PEMFCs experience structural and chemical degradation at elevated temperatures. This section outlines the challenges faced by operating PEMFCs at high temperature.

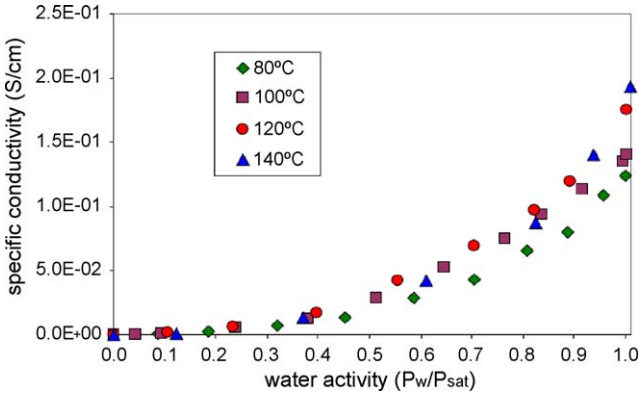

Fig. 7. Conductivity of Nafion 115 as a function of water activity at various temperatures [52].

3.1. Membrane conductivity and degradation

Typical proton-exchange membranes based on hydrated sulfonic acids dehydrate at elevated temperature or lower RH. As shown in Fig. 7, the conductivity of Nafion 115 drops significantly with a decrease in water activity at elevated temperatures (80–140 °C) [52]. It is therefore important to determine the influence of high temperature/low RH conditions on the conductivity of existing and emerging membranes so that limitations of operation may be identified.

Perfluorosulfonic acid (PFSA) membranes (e.g., Nafion) are the most widely used membrane for PEM fuel cells. Even these relatively robust materials lose their mechanical attributes when dehydrated, resulting in shrinking, and cracking. This accelerates gas crossover—with dire consequences to the cell's performance. Crossover also compromises safety since H_2 and O_2 may combine exothermically on Pt catalyst generating local hot spots that lead to pinholes, which in turn accelerates gas crossover—initiating a destructive cycle of increased crossover and membrane degradation.

A loss of mechanical stability with increasing temperature is to be expected in the fuel cell. Unfortunately, the failure mechanism of membranes in the fuel cell is not well understood. However, extensive morphological relaxation occurs above the glass transition temperature (T_g) of a polymer, which may have an adverse effect on properties of the membrane [53]. The glass transition temperature of the membrane must be well above the operating temperature of the fuel cell. T_g of hydrated samples is dependent on not only chemical structure of polymer but also water content due to its plasticizing effect. Nafion® has a T_g between 130 and 160 °C for the dry membrane, and between 80 and 100 °C for the hydrated membrane.

Several studies have addressed the issue of thermal stability of PFSA membranes. The PTFE like backbone of Nafion® is relatively stable due to the C–F bond strength and the shielding effect of the electronegative fluorine atoms. Nafion® begins to decompose via its side chains. Surowiec and Bogoczek [54] conducted a study using thermal gravimetric analysis (TGA), differential thermal analysis, and infrared spectroscopy, and concluded that Nafion® loses only water below 280 °C, while above 280 °C sulfonic acid groups are lost. Chu et al. [55] used infrared

spectroscopy to study the effect of heating Nafion® coated onto platinum in air and concluded that Nafion® loses sulfonic acid groups after being heated at 300 °C for 15 min. Wilkie et al. [56] using TGA and FTIR spectroscopy, reports that, while being heated between 35 and 280 °C in an inert atmosphere, Nafion® loses ∼5 wt.%, producing water and small amounts of sulfur dioxide and carbon dioxide. Between 280 and 355 °C, the evolution of sulfur dioxide and carbon dioxide increased. Detailed mechanisms for the decomposition of Nafion® are reported [56].

During fuel cell operation, it is believed that radicals HOO• and HO• are responsible for chemical attack on the membrane, and initiate the degradation process [57,58]. Water in the membrane provides a pathway for hydrogen and oxygen crossover from opposite sides of the membrane. Diffusion rates are slow and generally represent only a 1–3% loss in fuel cell efficiency; however, oxygen crossover provides a means for the formation of peroxide and hydroperoxide radicals, which may slowly deteriorate the membrane. Consequently, the loss of ionic groups has been observed to begin at the anode side of the membrane and progresses towards the cathode [59]. All these degradation processes are expected to be exacerbated at temperatures >100 °C, so that any consideration of new membranes for high temperature operation must be based on highly stable components, or engineered in a way to reduce free radical formation.

3.2. Degradation of the gas diffusion electrode

Development of durable, cost-effective gas diffusion electrodes for high temperature operation represents a significant challenge. Currently, noble metals such as Pt and Pt-alloys are used as electrocatalysts in PEMFCs. In order to improve Pt utilization and reduce Pt loading, noble metals are often supported on high surface area carbon substrates. Carbon supports provide a relatively large surface area for the electrocatalyst and provide good electronic conductivity.

It is recognized that long-term catalyst layer stability, even for cells operating at below 100 °C, is an area of concern. The issue of chemical and morphological instability of the catalyst layer is of greater concern at elevated temperatures. Firstly, corrosion of the carbon support in the cathode may occur if the cathode is held at relatively high oxidation potentials because of the generation of oxygen atoms at the catalyst. At elevated temperature, these may react with the carbon substrate and/or water to generate gaseous products such as CO and CO_2. This may destroy the carbon support over time, leading to a reduction in carbon content within the catalyst layer, thus, decreasing the cell lifetime. The carbon–oxidation reaction is influenced by the temperature, interfacial electrode potential and vapor pressure of water. It has been reported that this reaction is first order with respect to the water vapor. The oxidation rate of carbon is higher at higher electrode potentials. Experimental verification of this is provided by Stevens and Dahn [60] who studied the thermal degradation of carbon-supported Pt and found that the rate of carbon corrosion increased with Pt loading and temperature as shown in Fig. 8.

Another issue is agglomeration of Pt particles and the increase in particle size during PEMFC operation—a process that is exacerbated at elevated temperatures [61,62]. The rate of ORR on Pt/C catalyst has been demonstrated to be strongly dependent on the particle size [63–65]. The optimum particle size for ORR activity is 3–5 nm [62]. Due to the increase of Pt particle size over time the rate of ORR gradually decreases and Pt utilization is reduced. Pt is also observed to dissolve and re-deposit during long-term operation [66,67]. Two mechanisms are proposed for Pt dissolution [66]: electrochemical dissolution of Pt to Pt^{2+} according to the following reaction:

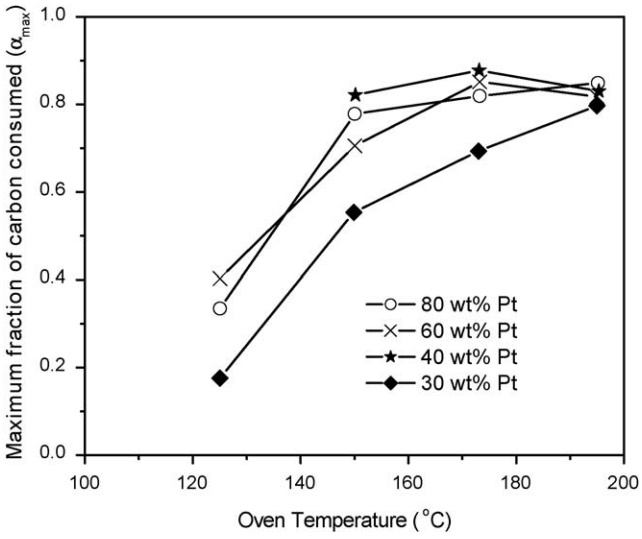

Fig. 8. Maximum fraction of carbon consumed as a function of temperature for samples with 30–80 wt.% Pt [60].

$$Pt = Pt^{2+} + 2e^- \quad (18)$$

and formation of Pt oxide film, followed by dissolution according to reactions (19) and (20). Irrespective of the actual mechanism in effect, the Pt particle's structure and location changes over time:

$$Pt + H_2O = PtO + 2H^+ + 2e^- \quad (19)$$

$$PtO + 2H^+ = Pt^{2+} + 2H_2O \quad (20)$$

It is necessary to develop high Pt content electrocatalysts to meet the requirements of operation at high temperatures and to reduce the cathode Pt loading. A combination of higher activity catalysts and thinner catalyst layers is required to achieve acceptable FC performance. A high Pt loading catalyst is needed to prepare thinner catalyst layers while maintaining the adequate PEMFC performance.

3.3. Relative humidity and humidification issues

Relative humidity (RH) is given by the ratio of the vapor pressure, $P(T)$, to the saturation vapor pressure (P_{sat}) multiplied by 100 [68]. It is related to temperature and pressure. The saturated vapor pressure P_{sat} is empirically described by Eq. (21) [68] and Eq. (22) [69]:

$$\ln P_{sat} = 21.564 - \frac{5420}{T} \quad (21)$$

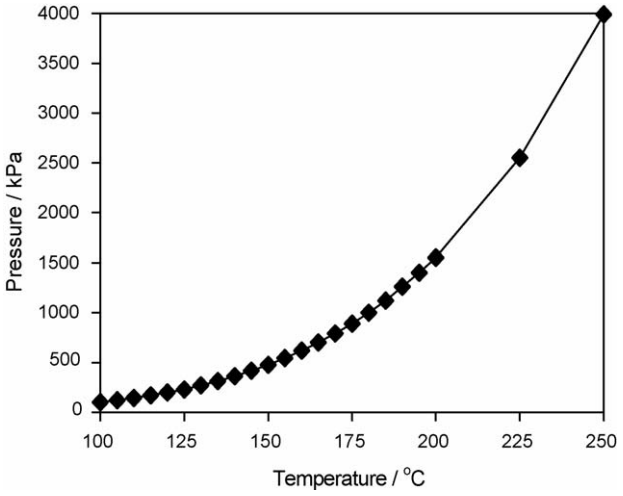

Fig. 9. Saturated water vapor pressures vs. temperature [70].

$$\ln P_{sat} = A - \frac{B}{T} \tag{22}$$

where A and B are constants. The saturated water vapor pressure increases exponentially with temperature, as shown in Fig. 9 [70].

As can be observed from Fig. 9, at temperature of 180 °C, the pressure P_{sat} reaches 10 atm. To maintain 100% RH at this temperature requires a total pressure of >10 atm; this without even considering the partial pressure of fuel and oxidant gases. The total pressure must also be comprised of the partial pressures of fuel and oxidant gases otherwise this will lead in an increased concentration overpotential. At a partial pressure of 0.5 atm of the reactant gases, for example, in a water-saturated feed stream designed to maintain 90% RH at 150 °C, this requires a total pressurization of >8 atm [1].

A system operation pressure is represented by the maximum flow rate of wet reactant gases it can provide. The hydrogen and air usages V_{H_2} and V_{air} (std l min^{-1}) in PMFECs are given by the following equations [71]:

$$V_{H_2} = 0.0076\lambda \frac{p_e}{V_c} \tag{23}$$

$$V_{air} = 0.0182\lambda \frac{p_e}{V_c} \tag{24}$$

where P_e is the power of fuel cell, V_c the single cell voltage and λ is the stoichiometric ratio. The gas usage increases linearly with the fuel cell power output, so the hydrated air and hydrogen flow rate increases linearly with fuel cell power output. Water consumption also increases. Thus, high flow rate of water vaporization is essential to fuel cell operation in the high current density regime. If the same gas relative humidity is kept at high operation temperature, the operation pressure will increase. The typical pressure limitation for conventional PEM fuel cell is usually <4 atm, and under this pressure, the boiling point of water is about 145 °C. So at high operational temperature, it is difficult to provide wet gases with high relative humidity in a traditional fuel cell control system. Higher pressures are helpful to get wet gases with high relative humidity but high pressures will impinge on the lifetime of the humidifier.

There are two conventional methods used to humidify fuel cell reactants and the fuel cell membrane: external and internal [72]. The simplest is the external method and involves passing the gases through a temperature-controlled, water-filled container. This method works well with low gas flow rates (low fuel cell power conditions). Internal humidification requires injecting water directly into the gas line leading to the fuel cell. This type of humidifier is compact and metering the liquid water into the gas stream can be easily controlled. Because the energy needed for vaporization is smaller at high temperature, injected water is more readily vaporized in the gas line. Internal humidification may be a preferred method for high temperature FC operation. If a membrane is employed that does not rely on water for proton conductivity then humidification is not necessary. Thus, the humidifier can be removed, the fuel cell system will be simplified, and the overall cost and efficiency will be improved.

3.4. Degradation of engineering materials and mechanical failure

Most of the materials that comprise a fuel cell system are in contact with water and oxygen at elevated temperatures. They are therefore subject to degradation or other oxidation processes. Material degradation is not restricted to MEA components, but includes seals, gaskets, and bipolar plates. The rates of which are increased at elevated temperature. The current collector plates and bipolar plates serve multiple functions including: current collection, gas distribution, water transport, thermal management, and humidification. For single cells, one side of the plate dictates the flow path for reactants from the inlet to the outlet manifold, while the other guides coolant flow or reactant. In fuel cell stacks, the bipolar plates are in contact with fuel and oxidant directly, and at high temperature. Bipolar plates are therefore subject to oxidizing conditions on one side and reducing conditions on the other. The dual requirement of good electrical conductivity and good resistance to corrosion over a range of oxidizing potentials severely restricts the choices of suitable bipolar plate materials. Under conditions of high temperature and high pressure, the rate of corrosion will increase. Products of corrosion are released into the fuel cell stack and may permeate MEAs. If the plates contain trace metals, metal ions accumulate in the membrane and catalyst layer reducing the protonic conductivity of these components. Protective coatings, such as oxides, may improve corrosion resistance but contribute to the contact resistance between the bipolar plate and the electrodes.

3.5. Heating strategies

An important consideration in high temperature FC operation is thermal management—raising the temperature to elevated levels and accurately maintaining the temperature. A method to obtain the uniform thermal distributions for fuel cell systems is to heat the fuel cell and gas lines in temperature environment such as an environmental chamber. However, small temperature differences between the cell and environment in the chamber

environment may cause heat rejection fro fuel cell reactions difficult; this will impair the thermal management of fuel cells at elevated temperature. Moreover, the oven is required to be explosion-proof because of the use of hydrogen. Alternatively, fuel cells can be placed in an ambient environment and the components heated individually. This provides a more rapid and controlled means by which to reject waste heat more quickly because of the larger temperature difference between the fuel cell component and the ambient surroundings.

4. Part III: progress towards high temperature operation

4.1. Membranes

The design of proton conducting membranes those are stable and provide good performance above 100 °C presents a major challenge. At high temperature and low humidity operation conventional PFSA membranes dehydrate and their conductivity decreases dramatically. The conductivity of Nafion 117 at 100% RH increases from 0.1 to 0.2 S cm^{-1} when the temperature is raised from 30 to 85 °C [73] but at 30 °C it decreases from 0.066 to 0.00014 S cm^{-1} as RH decreases from 100% to 34% [74]. Much effort has been made [75–81] to develop polymer membranes capable of retaining high proton conductivity in anhydrous environments, in addition to possessing chemical and electrochemical stability at high temperature. These developments can be classified into three groups [1]: (1) modified PFSA membranes, which incorporate hydroscopic oxides and solid inorganic proton conductors; (2) sulfonated polyaromtaic polymers and composite membranes, such as PEEK, SPEEK, SPSF, and PBI; (3) acid–base polymer membranes, such as phosphoric acid-doped PBI. Several review papers [1,82–85] already exist on the subject so only a cursory summary is provided here.

PFSA membranes may be readily modified by incorporating inorganic compounds, such as SiO_2 [86–88] and TiO_2 [88] into the hydrophilic domains in order to form nano-composite materials, and to improve their mechanical strength, thermal stability and water retention at elevated temperatures. Two methods are employed to prepare composite membranes: (1) direct addition of particles to a solution of Nafion, followed by casting; (2) impregnation of membranes with solutions of inorganic precursors, such as tetraethoxysilane, titanium tetraethylate, and in situ sol–gel reaction to produce a metal oxide. The fuel cell performance of several modified SPFA membranes are summarized in Table 1.

Another approach to high temperature membranes relies on the sulfonation of thermally resistant polymers such as sulfonated polyetheretherketones (SPEEK) [75,99,100], polyimides (PI) [101,102], polysulfones (PSF) [103,104], and poly

Table 1
Fuel cell performance of modified SPFA membranes

Membranes	Fuel cell conditions ($T_{anode}/T_{cell}/T_{cathode}$/pressure)	Performance	Reference
Nafion 112	90/100/90 °C, ambient pressure, H_2/air 90/120/90 °C, ambient pressure, H_2/air	0.69 V, 400 mA cm^{-2} 0.58 V, 400 mA cm^{-2}	[89]
Nafion 115/SiO_2 (6%)	130/130/130 °C, 3 bar, H_2/O_2 130/140/130 °C, 3 bar, H_2/O_2	0.4 V, 1000 mA cm^{-2} 0.4 V, 400 mA cm^{-2}	[90]
SDF-F/SiO_2 (4%)	108/110/108 °C, 2 bar, H_2/O_2 113/120/113 °C, 2.5 bar, H_2/O_2	0.6 V, 800 mA cm^{-2} 0.6 V, 700 mA cm^{-2}	[91]
Nafion/SiO_2/PWA[a] Nafion/SiO_2 Nafion/WO_3 Nafion/TiO_2	100/110/100 °C, 1.4 bar, H_2/O_2	0.4 V, 540 mA cm^{-2} 0.4 V, 320 mA cm^{-2} 0.4 V, 300 mA cm^{-2} 0.4 V, 185 mA cm^{-2}	[88]
Nafion 115/ZrP Recast Nafion 115/ZrP	130/130/130 °C, 3 bar, H_2/O_2 130/130/130 °C, 3 bar, H_2/O_2	0.45 V, 1000 mA cm^{-2} 0.45 V, 1500 mA cm^{-2}	[92]
ZrP/Nafion 115 composite	130/120/130 °C, 3 bar, H_2/O_2 130/130/130 °C, 3 bar, H_2/O_2 130/140/130 °C, 3 bar, H_2/O_2	0.6 V, 610 mA cm^{-2} 0.6 V, 530 mA cm^{-2} 0.6 V, 200 mA cm^{-2}	[52]
Nafion/PTA-I Nafion/PTA-II	90/120/90 °C, 1 bar, H_2/air	0.6 V, 120 mA cm^{-2} 0.6 V, 60 mA cm^{-2}	[93,94]
Mordenite/Nafion	90/110/90 °C, H_2/O_2, atmospheric pressure 90/120/90 °C, H_2/O_2, atmospheric pressure 90/130/90 °C, H_2/O_2, atmospheric pressure	0.6 V, 280 mA cm^{-2} 0.6 V, 110 mA cm^{-2} 0.6 V 0.6 V, 80 mA cm^{-2}	[95,96]
Nafion-Teflon-Zr(HPO_4)	87/105/91 °C, H_2/O_2 87/105/91 °C, H_2/air 87/120/91 °C, H_2/O_2 87/120/91 °C, H_2/air	0.6 V, 690 mA cm^{-2} 0.6 V, 350 mA cm^{-2} 0.6 V, 400 mA cm^{-2} 0.6 V, 200 mA cm^{-2}	[97]
15% SO_4^{2-}–ZrO_2/Nafion	110/120/110 °C, 3 bar, H_2/O_2	0.6 V, 1500 mA cm^{-2}	[98]

[a] Phosphotungstic acid.

Table 2
Summary of inorganic–organic composite membranes [1]

Organic component	Inorganic component	Comments	Reference
SPEK, SPEEK	ZrP + (SiO_2, TiO_2, ZrO_2)	Reduced methanol crossover	[238]
SPEEK	SiO_2, ZrP, Zr-SPP	0.09 S cm^{-1} at 100 °C, 100% RH, H_2/O_2 fuel cell test at 95 °C	[27]
SPEEK	HPA	10^{-1} S cm^{-1} above 100 °C	[225]
SPEEK	BPO_4	5×10^{-1} S cm^{-1} at 160 °C, fully hydrated	[239]
SPEEK	SiO_2	(3–4) $\times 10^{-2}$ S cm^{-1} at 100 °C, 100% RH	[240]
SPSF	PWA	0.15 S cm^{-1} at 130 °C, 100% RH	[241]
SPSF	PAA	0.135 S cm^{-1} at 50 °C, 100% RH	[237,242]
SPSF	PAA	2×10^{-2} S cm^{-1} at 80 °C, 98% RH	[214]
SPSF	PAA	H_2/O_2 cell, 500 h at 80 °C and 4 atm	[215]
PBI	ZrP + H_3PO_4	9×10^{-2} S cm^{-1} at 200 °C, 5% RH	[243]
	PWA/SiWA + H_3PO_4	(3–4) $\times 10^{-2}$ S cm^{-1} at 200 °C, 5% RH	
PBI	SiWA + SiO_2	2.2×10^{-3} S cm^{-1} at 160 °C, 100% RH	[234]
PBI	PWA + SiO_2 + H_3PO_4	T_d > 400 °C; 1.5×10^{-3} S cm^{-1} at 150 °C, 100% RH	[233]
PVDF	SiO_2, TiO_2, Al_2O_3, doping acids	>0.2 S cm^{-1} at 25 °C	[244]
		>0.45 S cm^{-1} at 25 °C, DMFC at 80 °C	[245]
PVDF	CsHSO4	10^{-2} S cm^{-1} at >150 °C, 80% RH	[130]
PVDF-SPS	AA	High-dimensional stability	[246]
GPTS	SiWA + SiO_2; SiWA + ZrP	1.9×10^{-2} S cm^{-1} at 150 °C, 100% RH	[247]
ICS-PPG	PWA, SiWA, and W-PTA	10^{-6} to 10^{-3} S cm^{-1}	[248]
Polysilsesquloxanes	PWA	3×10^{-2} S cm^{-1} at 140 °C	[249]
ORMOSIL	HPA	10^{-3} S cm^{-1} at 25 °C, DMFC test	[250]
PEO	Tungsten acid	10^{-2} S cm^{-1} at 120 °C; 1.4×10^{-2} 80 °C	[230]
PEO, PPO, PTMO	PWA	T_d = 250 °C; 10^{-2} S cm^{-1} at 140 °C	[231,232]
PVA/glycerin	ZrP + AA	10^{-3} to 10^{-4} S cm^{-1} at 25 °C; T_d > 110 °C	[251]
PTFE	Zeolites	DMFC test	[252]
PTFE	ZrP	4×10^{-2} S cm^{-1}	[253,254]

(*p*-phenylene) [105]. Some of these polymers yield membranes that are less dependent on humidity than PFSIs if their associated H_2O/SO_3^- values (lambda) are lower. This allows for good proton conductivity and good fuel cell performance at elevated temperatures. Li et al. [1] have summarized the development of this class of polymer in inorganic–polymer composite membranes. As shown in Table 2, some of these composite membranes exhibit promising conductivities at elevated temperatures. However, the performance of most has not been reported in operating fuel cells.

The third approach to achieving proton conductivity in membranes at high temperature is to replace water with another proton transport assisting solvent that possesses a higher boiling point, e.g., phosphoric acid and imidazoles. Poly(2,5-benizimidazole) (ABPBI) membranes prepared by simultaneously doping and casting from a solution of poly(2,5-benzimidazole)/phosphoric acid/methanesulfonic acid (MSA) contained up to 3.0 H_3PO_4 molecules per ABPBI repeating unit, and gave a maximum conductivity of 1.5×10^{-2} S cm^{-1} at temperatures as high as 180 °C under dry conditions [106]. Phosphoric acid-doped polybenzimidazole (PBI) has also been incorporated with inorganic proton conductors such as zirconium phosphate (ZrP, $Zr(HPO_4)_2 \cdot nH_2O$) [107], phosphotungstic acid (PWA, $H_3PW_{12}O_{40} \cdot nH_2O$) [107,108] and silicotungstic acid (SiWA, $H_4SiW_{12}O_{40} \cdot nH_2O$) [109]. Proton conductivities are found to be dependent on the acid doping level, relative humidity (RH) and temperature. A conductivity of 6.8×10^{-2} S cm^{-1} is observed for PBI membranes with a H_3PO_4 doping level of 5.6 (H_3PO_4 per repeat unit of PBI) at 200 °C and 5% RH. A higher conductivity of 9.6×10^{-2} S cm^{-1} is obtained for composites containing 15 wt.% of ZrP under the same conditions [107]. Acid-doped PBI membranes possess good performance at elevated temperature, even at 200 °C. The reported performance of several acid–base polymer membranes is summarized in Table 3.

For commercial viability fuel cell must demonstrate durability and reliability. For automotive applications, systems must exhibit a lifetime of >5000 h (temperature cycle resistance > 30,000 h); while for stationary power, 40,000 h must be demonstrated (temperature cycle resistance > 4000 h) [115,116]. There are numerous reports demonstrating the longevity of cells that operate below 100 °C, but there are few that address the longevity of high temperature fuel cells. Bauer et al. [117] performed a discontinuous test on SPEEK membranes at 90–110 °C for several days and found no degradation in performance. PBI polymeric electrolytes operating in fuel cells at temperatures above 100 °C have reported lifetimes of 3500 and 5000 h at 120 and 150 °C, respectively, under continuous operation [1]. To-date, the operational lifetime of high temperature fuel cells is far from satisfactory. During long-term operation at elevated temperature and low humidity membrane degradation is significant. Endoth et al. [118] found that membrane decomposition is more severe when operating under dry conditions than wet.

PFSA-based membranes show excellent thermal, chemical and mechanical stability in operating PEMFCs at 80 °C but instability is compromised at >120 °C [1]. Nafion membranes are stable ex situ up to 280 °C [119] at which temperature they undergo desulfonation. Some other classes of sulfonated

Table 3
Single cell PEMFC data of acid-doped PBI membranes

Membranes	Testing conditions ($T_{anode}/T_{cell}/T_{cathode}$/pressure)	Performance	Reference
H_3PO_4/PBI	190, 170, 150, and 100 °C, H_2/O_2, atmospheric pressure	0.6 V, 630, 430, 300, and 160 mA cm^{-2}	[110]
H_3PO_4/PBI	150 °C, H_2/O_2, atmospheric pressure	0.54 V, 250 mA cm^{-2}	[111]
	150 °C, H_2/air, atmospheric pressure	0.41 V, 250 mA cm^{-2}	
H_3PO_4-SPSF/PB	170 °C, H_2/O_2, 1 bar	0.6 V, 350 mA cm^{-2}	[112]
	130 °C, H_2/O_2, 1 bar	0.6 V, 180 mA cm^{-2}	
H_3PO_4-SPSF/PBI	200 °C, H_2/O_2, atmospheric pressure	0.6 V, 700 mA cm^{-2}	[113]
	200 °C, 3% CO–H_2/O_2, atmospheric pressure	0.6 V, 570 mA cm^{-2}	
H_3PO_4-SPSF/PBI	190 °C, H_2/O_2, 1 bar	0.6 V, 430 mA cm^{-2}	[114]

polymer exhibit higher thermal stability, for instance, methylbenzenesulfonated polymers are stable up to 370 °C [120], and alkylsulfonated polymers up to 400 °C [121]. Acid–base blended polymer membranes exhibit an even better thermal stability than covalently cross-linked ionomer membranes [85,103]. Although these thermal stability results show some promise for attaining high temperature membranes, they cannot be solely used to predict the long-term durability in operating fuel cells. Furthermore, the chemical stability of membranes at elevated temperature in oxidizing and reducing environments is also important in considering the durability of HT-PEMFCs. It is believed that the radical species attack the polymer chain leading to degradation of the membrane.

In summary, relatively little is published with regards to durability—even for low temperature PEMFCs. PEMFC durability has remained a difficult topic to study because of long testing periods; the complexity of analytical techniques to evaluate failure at the molecular level; the overlapping root causes of failure; and the absence of meaningful, in situ, non-destructive analyses. These difficulties are exacerbated when attempting study PEMFCs and fuel cell components at elevated operating temperature and lower humidity.

4.2. Catalyst layer and MEA compositions

There are two conventional approaches to fabricate catalyst layers and MEAs. In one method [122,123], a slurry containing electrocatalyst, ionomer and PTFE is deposited on a gas diffusion layer such as carbon paper. Two sheets of this catalyst-coated GDL are used to sandwich the membrane, and good contact is achieved by hot-pressing. In this type of MEA, it may be difficult to establish the desired ionic contact between the electrodes and the membrane and interfacial resistance may be higher than acceptable. In a second approach, the catalyst-coated membrane (CCM) method [124,125], the slurry of electrocatalyst is coated directly onto a proton conducting membrane or first onto an inert material, such as PTFE, before transferring to the membrane. The latter provides good adhesion between the membrane and catalyst layers, which decreases the interfacial resistance and improves Pt utilization and PEMFC performance.

A decrease in proton conductivity in the membrane, catalyst layer, and membrane/catalyst layer interface is expected to be the main limitation with high temperature operation. The catalyst-coated membrane (CCM) technique may be a better approach for preparing MEAs for HT-PEMFC because the catalyst layer can be made thinner, the catalyst loading can be reduced, and adhesion between the catalyst layer and membrane is improved. Song et al. [89,126] prepared MEAs using Nafion 112 and Nafion-Teflon-phosphotungstic acid membranes using the CCM technique and obtained high PEMFC performance at elevated temperature and low relative humidity. Polarization curves for a hydrogen/air cell at three operating conditions are shown in Fig. 10. The cell delivered 400 mA cm^{-2} for voltages as high as 0.72 V under the conditions stated. Bonville et al. [127] similarly fabricated MEAs using the CCM technique with Nafion-PTFE-PTA membranes and achieved good performance at elevated temperature and low relative humidity.

Nafion ionomer in the catalyst layer dehydrates and loses proton conductivity at high temperature and/or lower relative humidity. Although attention is being paid to the conductivity of bulk membranes at elevated temperature less work is devoted to the effect of dehydration of the catalyst layer. New ionomer materials for high temperature PEM fuel cells must be readily fabricated into well-bonded, robust membrane electrode assemblies. Novel ionomers must also be adaptable and have the necessary physical strength and ductility in the dry and wet states. Both the ionomer in the membrane and in the GDE should

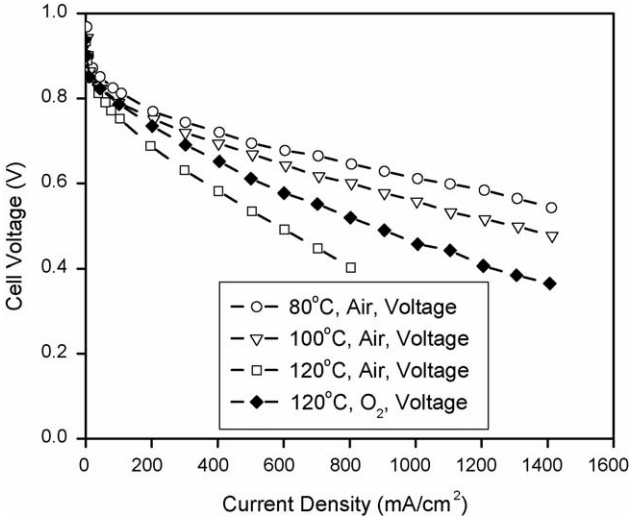

Fig. 10. Polarization curves from MEAs prepared by the CCM technique (Nafion 112). The three operating conditions are (cell temperature/anode RH/cathode RH) 80/100/75, 100/70/70, and 120/35/35, ambient pressure [89].

have the capacity to either retain moisture or conduct protons in the absence of liquid water.

Higuchi et al. [128] prepared gas diffusion electrodes for high temperature operation by using a proton conductive borosiloxane (BSO) electrolyte. The catalyst layer composed of Pt supported on carbon black (Pt-CB) and BSO ionomer. The polarization properties and the microstructure of the catalyst layer were investigated as a function of BSO/CB mass ratio. A performance of 0.6 V at 600 mA cm^{-2} was achieved at BSO/CB = 1.5 (w/w) at 80 °C with 0.43 mg cm^{-2} Pt loadings for both cathode and anode. Nishikawa et al. [129] prepared GDEs using new organic/inorganic hybrid electrolytes. Catalyst layers were prepared by mixing 3-(trihydroxysilyl)-1-propanesulfonic acid [(THS)pro-SO_3H], 1,8-bis(triethoxysilyl) octane (TES-Oct), Pt/carbon and water, followed by a sol–gel reaction. This MEA was tested at 80 °C with humidified H_2 and dry O_2 under ambient pressure. The catalyst layer exhibited a performance similar to Nafion-based systems.

There is also reported activity in the industrial sector in the pursuit of high temperature MEAs. PEMEAS GmbH [130] report the performance of a MEA prepared using Celtec®-P 1000—a phosphoric acid-doped PBI membrane. These MEAs may be operated from 160 to 200 °C, preferably 160–180 °C. A lifetime of >14,000 h is reported at 160 °C using hydrogen and air under ambient pressure. A CO tolerance of 0.1% is reported. Polarization curves are shown in Figs. 11 and 12 [130]. PEMEAS Fuel Cell Technologies, E-TEK Division [131] also supplies commercial gas diffusion electrodes for high temperature PEM fuel cells. These GDEs may be operated at temperatures above 95 °C.

In 2004 Asahi Glass Co., Ltd. [132] announced that it had increased the durability of its propriety fluorinated, proton conducting polymer-based MEA (Aciplex®). According to the company, the rate of MEA degradation is lowered by a factor of 10 compared to state-of-the-art MEAs, and has logged >2000 operational hours at 120 °C.

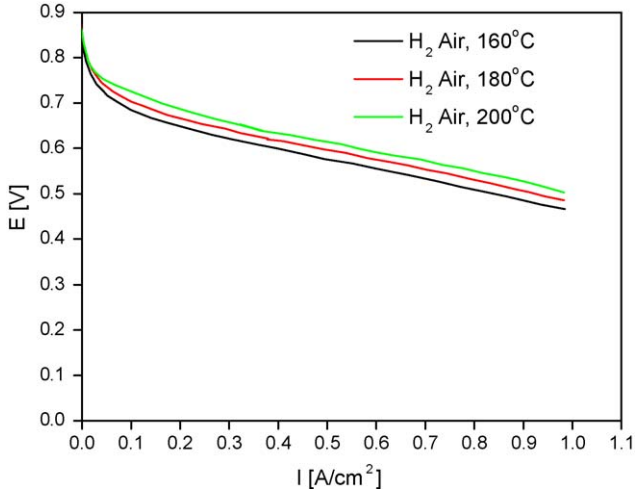

Fig. 11. Polarization curves for Celtec®-P1000-based MEAs using H_2/air [130]. Active cell area: 45 cm^2; air: stoichiometry = 2; 0 bar_g, H_2: stoichiometry = 1.2; 0 bar_g, humidification: none.

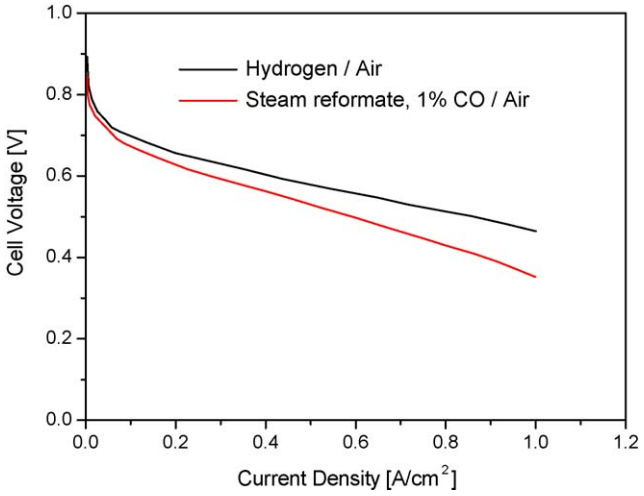

Fig. 12. Reference performance test data of Celtec®-P1000-based MEA under reformate conditions with high CO concentrations. Active area: 45 cm^2; temperature: 160 °C, ambient pressure, anode: stoichiometry = 1.2, cathode: stoichiometry = 2.0; reformate: 70% H_2, 29% CO_2, 1% CO [130].

4.3. Flow fields

The design of flow fields is a key factor in the operation and performance of PEMFCs. They provide channels for transporting reactant gases, liquid water and water vapor; the configuration, dimensional parameters, and aspect ratio significantly impact PEMFC performance. Sun et al. [133] investigated the impact of the flow field pattern on the gas concentration and performance of PEMFCs using parallel straight and serpentine flow field patterns, respectively, as shown in Fig. 13. They concluded that the gas concentration of the straight flow pattern appears excessively nonuniform, resulting in a local concentration polarization. However, the gas concentration is well distributed for the serpentine flow pattern, creating a better mass transfer phenomenon [133].

Li and Sabir [134] reviewed the impact of the design of several types of flow fields and presented their attributes and deficiencies. A pin-type flow field (Fig. 14(a)) was developed by Reiser and coworkers [135,136]. As stated by Li and Sabir [134], this type of flow field results in a low reactant pressure drop but reactants flowing through such flow fields tend to follow the path of least resistance, which may lead to channelling, the formation of stagnant areas, uneven reactant distribution, inadequate product water removal and poor fuel cell performance.

Pollegri and Spaziante [137] developed a parallel straight flow filed, as shown in Fig. 14(b), which includes a number of parallel flow channels connected to gas inlet and outlet. In this flow field, water produced at the cathode accumulates in channels and may block them. An interdigitated flow field (Fig. 14(c)) provides convection at the electrode surface in order to improve mass transfer. This flow-field design can help remove water effectively from the electrode, thereby preventing "flooding", but a large pressure loss occurs for the reactant gas flow, especially for the oxidant stream.

A single serpentine flow field [138,139] and a multiple serpentine flow field [140,141] are shown in Fig. 14(d) and (e),

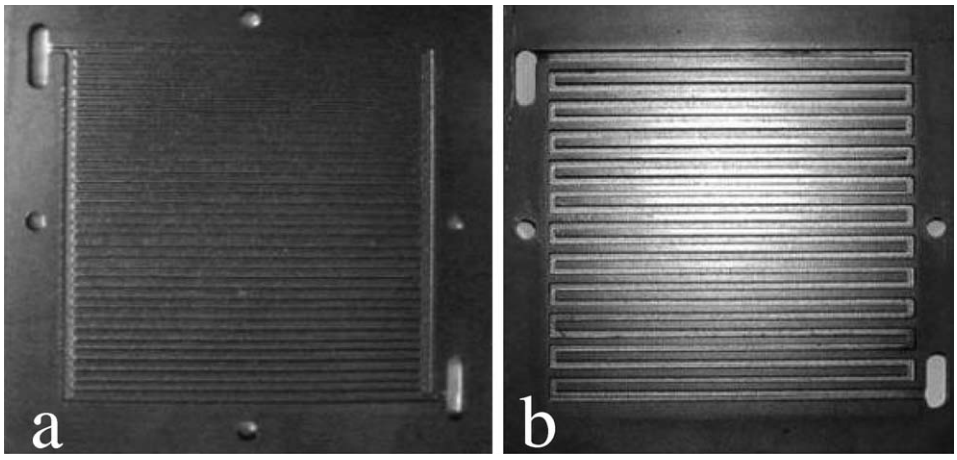

Fig. 13. Schematic illustration of different flow-field patterns [133]: (a) parallel straight pattern; (b) serpentine pattern.

respectively. As noted by Li and Sabir [134], the single serpentine flow field can force the reactant flow to traverse the entire active area of electrode. However, this design results in a relatively long reactant flow path, hence, a substantial pressure drop and significant concentration gradient from the gas inlet to outlet. In addition, it is difficult to remove water produced at the cathode. Although the multiple serpentine flow field ensures adequate water removal, mitigates stagnant area formation, and reduces the reactant pressure drop relative to single serpentine designs, the reactant pressure drop through each of the serpentines remains relatively high due to the relatively long path of each channel; thus, the reactant concentration changes significantly from the flow inlet region to the exit region.

Optimization of the flow-field design parameters should reduce or eliminate the accumulation of product water. Designing the flow field pattern to have a higher internal pressure drop will better remove excess liquid water from the fuel cell more efficiently, but for high temperature PEM fuel cells, water exists in the flow fields as vapor and "flooding" is less of a concern. Flow-field designs should therefore focus on decreasing the pressure drop and improving mass transfer by increasing the reactant concentration near MEAs.

The distribution of reactant along a channel is not uniform. When reactants are consumed, the concentration of reactants near the catalyst layer decreases, while the concentration of reaction products increases. Reactants with low concentration near the end of the flow field move slowly to the catalyst surface, which will reduce the performance of fuel cells operating at high current density. Similarly, the concentration of products near the catalyst surface can quickly reach saturation. Thus, mixing flu-

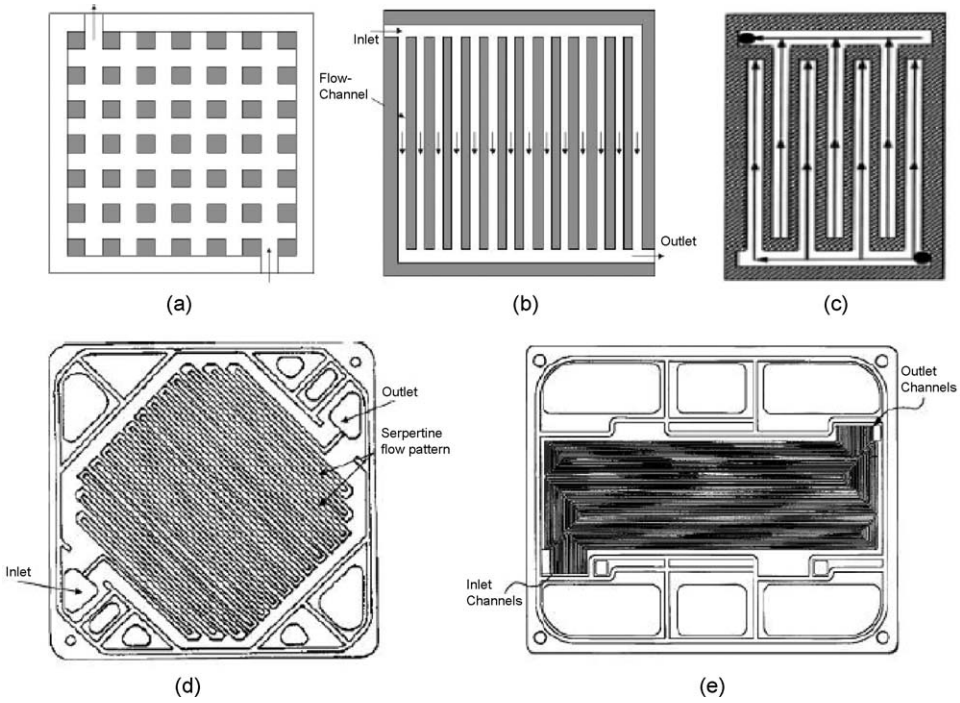

Fig. 14. Schematic of flow-field designs [134].

ids in channels and increasing reactant concentrations near the catalyst layers is helpful to improve the performance of high temperature fuel cells.

4.4. Fuel cell testing

Currently the majority of research activities in the area of HT-PEMFC focus on the development of high temperature membranes. There are few reports on technologies for characterizing and evaluating HT-PEMFCs. There are several issues associated with testing and diagnosis at elevated temperature, such as humidity control, thermal management, material corrosion, performance degradation, cell design, lifetime, all of which add to the complexity of analysis.

4.4.1. Test station

Fuel cell test stations are designed to control the following parameters: temperature, pressure, humidity and flow rates of reactant gases and coolant; and to measure cell current and voltage [142]. A test station consists of the following units: gas control station, load bank, data acquisition/control unit and control software [143,144]. Fig. 15 shows a schematic diagram of a test station.

The gas control station is used to regulate the gas velocity, temperature and relative humidity. A safety unit is added to detect and remove any explosive leaking gases from the test station. The load bank operates in several load modes: constant current, constant voltage, and constant power. A data acquisition/control unit monitors and controls all data from the test station and fuel cell system. Control software is used to monitor, control and organize the testing processes. Conventional test stations can be modified for HT-PEMFC testing. Fuel, oxidant, and the fuel cell may be heated to >100 °C through the use of external heating tubes and elements. However, the potentially higher pressure and higher humidity may create issues related to sealing, material fatigue and lifetime of the apparatus.

4.4.2. New set of fuel cell component materials

Compared to conventional fuel cells, the requirements of component materials for the HT-PEMFCs are more stringent because rates of corrosion and degradation are increased at elevated temperatures. It is essential to ensure adequate sealing of bipolar plates in order to avoid leakage of fuel and oxidant, and to provide good mechanical and electrical contact between the MEA and bipolar plates. O-rings are typically used in a fuel cell stack to prevent loss of gases. The mechanical and thermal properties of sealing materials such as compressibility, electrical properties, glass transition temperature, Young's modulus, and mechanical creep are just a few important considerations in O-ring selection. Table 4 lists the recommended operational temperature ranges of principal elastomers employed as seals [145]. For conventional fuel cells, there many materials that can be used for sealing, but the majority cannot be used at higher temperatures. If the fuel cell is intended to be operated above 180 °C, only those materials having a tolerance to >200 °C should be used, e.g., silicon rubber, tetrafluoroethylene-propylene (AFLAS®), perfluoroelastomer (FFKM), fluorocarbon (FKM), and ethylene propylene rubber (EPM, EPDM). The resistance of sealing materials to steam requires special consideration and new materials are being developed. For example, Parker [145] developed an ethylene propylene material that exhibited very little change in physical properties after 70 h exposure to steam at 288 °C.

In principle, any of the materials in the system in contact with an aqueous phase may be subjected to corrosion. The bipolar plate/current collector components, are of special concern, since they are exposed to fuel and oxidant directly at high temperature. They are subjected to oxidizing conditions on one side and reducing conditions on the other. The dual requirement of good electrical conductivity and good resistance to corrosion across a range of oxidizing potentials severely restricts the choice of suitable materials. The corrosion rate is affected not only by the electrochemical potential, but also by operating parameters and duty cycle placed on the FC stack. At high temperature and under high pressure, rates of corrosion are increased. Visual macroscopic signs of corrosion are the appearance of holes, cracks, and fissures that may cause the component to fail catastrophically. However, there are more subtle forms of corrosion-induced failure, such as the release of corrosion products that accumulate in the MEA. Cations, for example, are taken up by membranes, which reduce their proton conductivity. Corrosion products absorb onto the electrocatalyst reducing their function. An oxide film may accumulate on the bipolar plate

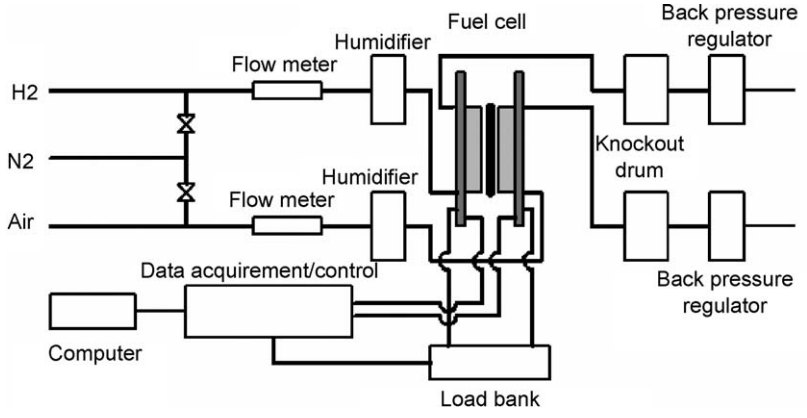

Fig. 15. Schematic of a test station.

Table 4
Useful temperature ranges of principal elastomers used in seals [145]

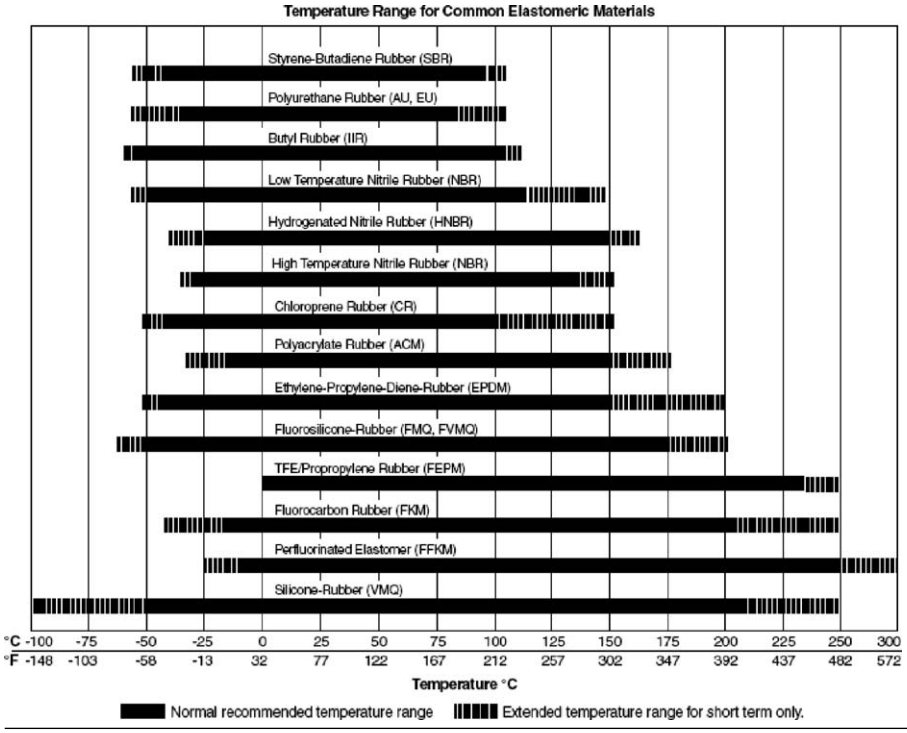

that may contribute to an increased contact and stack resistance. In conventional fuel cell, graphitic plates are often used; alternatives are stainless steel, titanium, coated aluminum and other alloys, but the more corrosive environment found in high temperature/high humidity operation may severely limit the range of useable bipolar plate materials.

4.5. Diagnostic technologies

Like any other device, it is necessary to know when and why a fuel cell is not operating to it full potential. Diagnostic information is required for testing and prototype development, components selection, and evaluation of emerging materials. Diagnostics is also very important for preventing damage to the device and peripheral instrumentation and for reasons of safety. Diagnostic technologies for low temperature PEM fuel cells are in a state of development, and these provide the basis for high temperature PEMFC diagnostics.

4.5.1. Linear and cyclic sweep voltammetry

The technique of linear sweep voltammetry (LSV) is used to evaluate and monitor fuel crossover and to check for the electronic shorts. Cyclic sweep voltammetry (CV) is used to determine electrochemical areas (ECA) of electrodes. In these methods ultra-high purity H_2 and ultra-high purity N_2 or He is passed over the anode and cathode, respectively. The anode is used as the reference and counter electrode; and the cathode is used as the working electrode. Song et al. [89] measured the hydrogen crossover through membranes and the Pt electrochemical surface area of the cathode in a HT-PEM fuel cell using LSV and CV, respectively (see Fig. 16). For the LSV, the sweep rate was 4 mV s^{-1} and the cell potential was scanned from 0 to 0.5 V. Hydrogen that passed through the membrane was measured as a mass transport "limiting current" at 0.35–0.5 V. For CV, the sweep rate was 20 mV s^{-1} and the cell was cycled between 0.0 and 0.8 V, however, both measurements were conducted at ambient temperature.

LSV has also been used to quantify hydrogen crossover and hydrogen permeation through a membrane at elevated temperatures, i.e., under HT-PEMFC operating conditions [146–148].

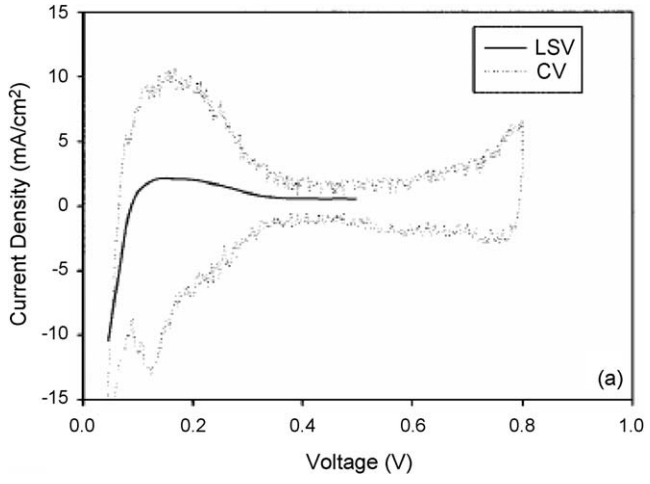

Fig. 16. LSV (4 mV s^{-1}, 0.01–0.50 V) and CV (20 mV s^{-1}, 0.01–0.80 V) at 25 °C, 200 cm^3 min^{-1} pure H_2 at the anode, and 200 cm^3 min^{-1} N_2 at the cathode of a single cell [89].

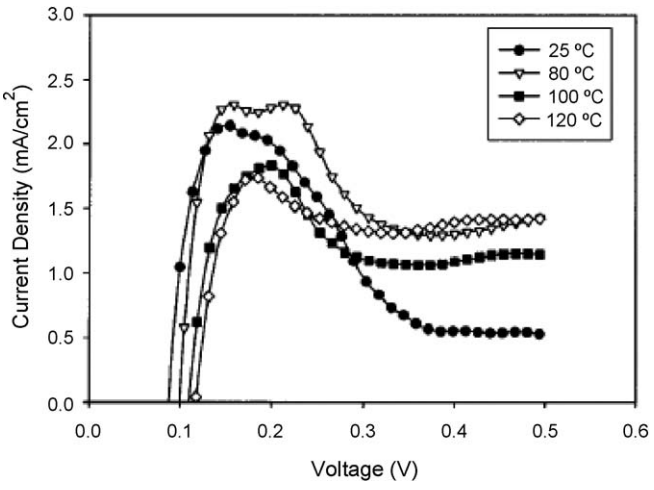

Fig. 17. LSV of cell 1 (4 mV s^{-1}, 0.01–0.50 V), 200 cm^3 min^{-1} pure H_2 on the anode, and 200 cm^3 min^{-1} N_2 on the cathode, at four conditions in comparison: 25/100/100, 80/100/75, 100/70/70, and 120/35/35 [89].

The increase in hydrogen crossover, via LSV is demonstrated in Fig. 17 [89].

The ECA of Pt in fuel cell cathode can be calculated based on the relationship between surface area and the charge associated with hydrogen adsorption on the electrode, as determined using CV. The hydrogen adsorption charge on a smooth Pt electrode is 210 $\mu C\,cm^{-2}$ Pt [149]. The ECA is calculated according to Eq. (25) [89,150], which can be used to calculate the utilization of Pt in the gas diffusion electrode according to Eq. (26). CVs may also be performed during FC operation and can be used to monitor the health of the electrodes in real time:

$$\text{ECA}\,(\text{cm}^2/\text{g}) = \frac{\text{charge}\,(\mu\text{C}/\text{cm}^2)}{210\,(\mu\text{C}/\text{cm}^2\,\text{Pt}) \times \text{catalyst loading}\,(\text{g Pt}/\text{cm}^2)} \quad (25)$$

$$\text{Pt utilization}\,(\%) = \frac{\text{ECA}}{\text{total Pt surface area}} \quad (26)$$

4.5.2. Electrochemical impedance spectroscopy (EIS)

Electrochemical impedance spectroscopy (EIS) is a powerful technique to characterize the kinetics of an electrode–electrolyte interface. Two main methods are used to measure impedance: time domain and frequency domain techniques. The frequency domain technique typically uses a potentiostat and a frequency response analyzer. The electrochemical potential of the working electrode is modulated sinusoidally with respect to the reference electrode. The impedance is a frequency dependent complex number that can be plotted in various ways, but is generally plotted in the complex plane. By fitting this impedance spectrum to a model or an equivalent circuit, an equivalent circuit for the system can be obtained.

EIS was traditionally applied to the determination of the double layer capacitance [151]. Now, EIS is used widely to characterize the electrical properties of materials and interfaces. Its application in PEMFCs diagnostics is well established and most of these methods are applicable to HT-PEMFCs. EIS has been used as a method for determining membrane conductivity and resistance. For example, Benavent et al. [152] characterized novel activated composite membranes by impedance spectroscopy and determined the electrical resistance of different membrane samples. Freire and Gonzalez [153] studied the effect of membrane characteristics and humidification conditions using the impedance response of polymer electrolyte fuel cells. It was shown that impedance spectroscopy is a powerful tool to investigate the effects of temperature, membrane thickness and operational conditions on the performance of PEMFC. The EIS of fuel cells may be complex but contains an abundance of information. For example, the impedance loop that is sometimes evident at mid-frequencies is due to double layer charging from the charge transfer resistance and the low frequency arc is caused by the gas-phase transport limitations [12,154–157]. CO tolerance of PEMFCs can also be characterized by EIS. Kim et al. [158] found that CO has a greater effect on the charge transfer reaction (high frequency arc) and hydrogen dissociative chemisorption (medium frequency arc), but little effect on the low frequency arc. They also found that CO gas has little effect on cathode impedance. At low temperature and high CO concentration, the fuel cell impedance depends on the anode impedance.

5. Conclusions

A literature review on HT-PEMFCs reveals that HT-membrane development accounts for ~90% of the papers. The rest of the literature covers issues of system modelling, evaporative cooling, catalyst performance, and vapor phase DMFC. Research articles discussing either HT-PEMFC design or HT-PEMFC test station design were notably absent. This does not mean work in this area does not exist—simply that it is often found in industrial research laboratories and is more likely to emerge in the form of a patent. A review of the patents literature again revealed a large number on membrane technologies and their associated fabrication methods. Numerous patents exist discuss techniques for operating fuel cells under low humidification, but very few describe HT-PEMFC architecture and design beyond the membrane.

Despite concentrated research efforts into membranes for high temperature/low humidity operation the status of the field is far from satisfactory. Membranes generally dehydrate under these conditions, thereby decreasing the performance of the fuel cell. A membrane, which transports protons using transport media that does not include water, is highly desirable. Some advances in this direction are emerging, e.g., the use of imbibed acids and N-containing heterocycles, but other issues need addressing. The discovery and development of a high temperature/low humidity membrane is widely considered to play a key role in the progress of HT-PEMFC technology.

In our view, a significant weakness in the development of HT-PEMFC technology is the deficiency in HT-specific fuel cell architectures test station designs, testing protocols, and a general under-developed understanding of testing and design protocols. The development of a HT-specific PEMFC design is of key importance and may help mitigate issues of membrane

dehydration and MEA degradation. Due to the higher rate of heat removal at high temperature, it may be possible to remove excess heat from the stack via the cathode airflow alone; thus simplifying the fuel cell stack, reducing its cost, and increasing its power density. Lastly, there is a strong need to research and investigate in situ and ex situ diagnostic technologies for HT-PEMFCs. A strong emphasis should be placed on ex situ analysis of HT-PEMFC related materials so that emerging and potentially technology-enabling materials may be rapidly examined and screened. In summary, the area of HT-PEMFCs is relatively immature, and requires significant research and discovery.

Acknowledgements

This work was financially supported by the NRC-National Fuel Cell Program, and the NRC-Institute for Fuel Cell Innovation. The contributions of Mr. Robert Chow, Ms. Lizhu Gu, and Mr. Tom Vanderhoek, Mr. Milos Sinuek and Mr. Andrew Mattie at NRC-IFCI are gratefully acknowledged.

References

[1] Q.F. Li, R.H. He, J.O. Jensen, N.J. Bjerrum, Chem. Mater. 15 (2003) 4896–4915.
[2] J.H. Jiang, A. Kucernak, J. Electroanal. Chem. 567 (2004) 123–137.
[3] C. Berger, Handbook of Fuel Cell Technology, Prentice-Hall, Inc., Englewood Cliffs, NJ, 1968.
[4] D.M. Bernardi, M.W. Verbrugge, J. Electrochem. Soc. 139 (9) (1992) 2477–2491.
[5] D.M. Bernardi, M.W. Verbrugge, AIChE J. 37 (1991) 1151–1163.
[6] H. Xu, Y. Song, H.R. Kunz, J.M. Fenton, J. Electrochem. Soc. 152 (9) (2005) A1828–A1836.
[7] A. Parthasarathy, C.R. Martin, S. Srinivasan, J. Electrochem. Soc. 138 (1991) 916–921.
[8] A.J. Appleby, B.S. Baker, J. Electrochem. Soc. 125 (1978) 404–406.
[9] A. Parthasarathy, S. Srinivasan, A.J. Appleby, C.R. Martin, J. Electrochem. Soc. 139 (1992) 2530–2537.
[10] A. Damjanovic, M.A. Genshaw, Electrochim. Acta 15 (1970) 1281–1283.
[11] A. Damjanovic, V. Brusic, Electrochim. Acta 12 (1967) 615–628.
[12] Z. Xie, S. Holdcroft, J. Electroanal. Chem. 568 (2004) 247–260.
[13] P.D. Beattie, V.I. Basura, S. Holdcroft, J. Electroanal. Chem. 468 (1999) 180–192.
[14] D.P. Wilkinson, D. Thompsett, in: O. Savadogo, P.R. Roberge (Eds.), Proceedings of the Second International Symposium on New Materials for Fuel-Cell and Modern Battery Systems, P266, Montreal, Canada, 1997.
[15] Z.Q. Qi, C.Z. He, A. Kaufman, J. Power Sources 111 (2002) 239–247.
[16] W. Vogel, L. Lundquist, P. Ross, P. Stonehart, Electrochem. Acta 20 (1975) 79–93.
[17] H.P. Dhar, L.G. Christner, A.K. Kush, J. Electrochem. Soc. 134 (1987) 3021–3026.
[18] H.P. Dhar, L.G. Christner, A.K. Kush, H.C. Maru, J. Electrochem. Soc. 133 (1986) 1574–1582.
[19] Q.F. Li, R.H. He, J.O. Jensen, N.J. Bjerrum, J. Electrochem. Soc. 150 (2003) A1599–A1605.
[20] G. Xiao, Q.F. Li, A.H. Hans, N.J. Bjerrum, J. Electrochem. Soc. 142 (1995) 2890–2893.
[21] C. Yang, P. Costamagna, S. Srinivasan, J. Benziger, A.B. Bocarsly, J. Power Sources 103 (2001) 1–9.
[22] J.B. Benziger, Thermochemical methods for reaction energetics on metal surfaces, in: E. Shustorovich (Ed.), Metal–Surface Reaction Energetics: Theory and Applications to Heterogeneous Catalysis, Chemisorption, and Surface Diffusion, VCH, 1991, pp. 53–108.
[23] K.T. Adjemian, S.J. Lee, S. Srinivasan, J. Benziger, A.B. Bocarly, J. Electrochem. Soc. 149 (2002) A256–A261.
[24] S. Malhotra, R. Datta, J. Electrochem. Soc. 144 (1997) L23–L26.
[25] R.J. Bellows, E.P. Marucchi-Soos, D.T. Buckley, Ind. Eng. Chem. Res. 35 (1996) 1235–1242.
[26] J.T. Wang, R.F. Savinell, J. Wainright, M. Litt, H. Yu, Electrochim. Acta 41 (1996) 193–197.
[27] B. Lakshmanan, W. Huang, D. Olmeijer, J.W. Weidner, Electrochem. Solid State Lett. 6 (12) (2003) A282–A285.
[28] T. Navessin, Ph.D. thesis, Simon Fraser University, Canada, 2004.
[29] K. Broka, P. Ekdunge, J. Appl. Electrochem. 27 (1997) 281–289.
[30] F. Jaouen, G. Lindbergh, G. Sundholm, J. Electrochem. Soc. 149 (2002) A437–A447.
[31] K.M. Yin, J. Electrochem. Soc. 152 (2005) A583–A593.
[32] M. Ise, K.D. Kreuer, J. Maier, Solid State Ionics 125 (1999) 213–223.
[33] T.A. Zawodzinski, J. Davey, J. Valerio, S. Gottesfeld, Electrochim. Acta 40 (1995) 297–302.
[34] T. Navessin, M. Eikerling, Q. Wang, D. Song, Z. Liu, J. Horsfall, K.V. Lovell, S. Holdcroft, J. Electrochem. Soc. 152 (2005) A796–A805.
[35] Z. Ogumi, Z. Takehara, S. Yoshizawa, J. Power Sources 131 (1984) 769.
[36] D.M. Bernardi, M.W. Verbrugge, AIChE J. 37 (1991) 1151–1163.
[37] S. Mitsushima, N. Araki, N. Kamiya, K. Ota, J. Electrochem. Soc. 149 (2002) A1370–A1375.
[38] K. Lee, A. Ishihara, S. Mitsushima, N. kamiya, K. Ota, J. Electrochem. Soc. 151 (2004) A639–A645.
[39] L. Zhang, C. Ma, S. Mukerjee, Electrochim. Acta 48 (2003) 1845–1859.
[40] L. Zhang, C. Ma, MukerjeeF S., J. Electroanal. Chem. 568 (2004) 273–291.
[41] K. Ota, Y. Inoue, N. Motohira, N. Kamiya, J. New Mater. Electrochem. Syst. 3 (2000) 193–197.
[42] P.D. Beattie, V.I. Basura, S. Holdcroft, J. Electroanal. Chem. 468 (1999) 180–192.
[43] Y.W. Rho, S. Srinivasan, J. Electrochem. Soc. 141 (1994) 2089–2096.
[44] R.S. Yeo, J. McBreen, J. Electrochem. Soc. 126 (1979) 1682–1687.
[45] J.S. Yi, T. Van Nguyen, J. Electrochem. Soc. 145 (1998) 1149–1159.
[46] C.Y. Wang, Chem. Rev. 104 (2004) 4727–4766.
[47] G. Frank, Proceedings of the Second European PEFC Forum P749, Lucerne, Switzerland, 2003.
[48] E. Cho, J.-J. Ko, H.Y. Ha, S Ahn Hong, K.Y. Lee, T.W. Lim, I.-H. Oh, J. Electrochem. Soc. 150 (2003) A1667–A1670.
[49] N.J. Fletcher, G.A. Boehm, E.G. Pow, US 5,798,186 (August 25, 1998).
[50] J.A. Roberts, J. St-Pierre, M.E. Van der Geest, A. Atbi, N.J. Fletcher, US 6,479,177 (November 12, 2002).
[51] J. St-Pierre, J. Roberts, K. Colbow, S. Campbell, A. Nelson, J. New Mater. Electrochem. Syst. 8 (2005) 167–176.
[52] C. Yang, S. Srinivasan, A.B. Bocarsly, S. Tulyani, J.B. Benziger, J. Membr. Sci. 237 (2004) 145–161.
[53] Y.S. Kim, F. Wang, M. Hickner, T.A. Zawodzinski, J.E. McGrath, J. Membr. Sci. 212 (2003) 263–282.
[54] J. Surowiec, Bogoczek, J. Therm. Anal. 33 (1988) 1097–1102.
[55] D. Chu, D. Gervasio, M. Razaq, E.B. Yeager, J. Appl. Electrochem. 20 (1990) 157–162.
[56] Z.A. Wilkie, J.R. Thomsen, M.L. Mittleman, J. Appl. Polym. Sci. 42 (1991) 901–909.
[57] F.N. Büchi, B. Gupta, O. Haas, G.G. Scherer, Electrochim. Acta 40 (1995) 345–353.
[58] H. Wang, G.A. Capuano, J. Electrochem. Soc. 145 (1998) 780–784.
[59] J.R. Yu, B.L. Yi, D.M. Xing, F.Q. Liu, Z.G. Shao, Y.Z. Fu, H.M. Zhang, Phys. Chem. Chem. Phys. 5 (2003) 611–615.
[60] D.A. Stevens, J.R. Dahn, Carbon 43 (2005) 179–188.
[61] M.S. Wilson, F.H. Garzon, K.E. Sickafus, S. Gottesfeld, J. Electrochem. Soc. 140 (1993) 2872–2877.
[62] T. Tada, High dispersion catalysts including novel carbon supports, in: Wolf Vielstich, Hubert, A. Gasteiger, Arnold Lamm (Eds.), Handbook of Fuel Cells-Fundamentals, Technology and Applications: Fuel Cell technology and Application, vol. 3, John Wiley and Sons, Ltd., 2003.
[63] K. Kinoshita, J. Electrochem. Soc. 137 (1990) 845–848.
[64] A. Kabbabi, F. Gloaguen, F. Andolfatto, R. Durand, J. Electroanal. Chem. 373 (1994) 251–254.
[65] S. Mukerjee, J. Appl. Electrochem. 20 (1990) 537–548.

[66] R.M. Darling, J.P. Meyers, J. Electrochem. Soc. 150 (2003) A1523–A1527.
[67] T. Patterson, Fuel Cell Technology Topical Conference Proceedings, AJChE Spring National Meeting, March 10–14, 2002.
[68] http://www.faqs.org/faqs/meteorology/temp-dewpoint/.
[69] W.A. Mark, H.D. Richard, Heat and Thermodynamics, 7th ed., McGraw-Hill, 1996.
[70] http://www.engineeringtoolbox.com/24_162.html.
[71] J. Larmine, A. Dicks, Fuel Cell Systems Explained, John Wiley & Sons, Ltd., New York, 2000.
[72] John P. Evans, Experimental evaluation of the effect of inlet gas humidification on fuel cell performance, Electronic Thesis, Mechanical Engineering, Virginia Polytechnic and State University, 2003.
[73] C. Ma, L. Zhang, S. Mukerjee, D. Ofer, B. Nair, J. Membr. Sci. 219 (2003) 123–136.
[74] A.V. Anantaraman, C.L. Gardner, J. Electroanal. Chem. 414 (1996) 115–120.
[75] B. Bauer, D.J. Jones, J. Roziere, L. Tchicaya, G. Alberti, M. Casciola, L. Massinelli, A. Peraio, S. Besse, E. Ramunni, J. New Mater. Electrochem. Syst. 3 (2000) 87–92.
[76] C. Yang, S. Srinivasan, A.S. Arico, P. Creti, V. Baglio, V. Antonucci, Electrochem. Solid State Lett. 4 (2001) A31–A34.
[77] G. Alberti, M. Casciola, R. Palombari, J. Membr. Sci. 172 (2000) 233–239.
[78] G. Alberti, M. Casciola, L. Massinelli, B. Bauer, J. Membr. Sci. 185 (2001) 73–81.
[79] M. Doyle, S.K. Choi, G. Proulx, J. Electrochem. Soc. 147 (2000) 34–37.
[80] R. Savinell, E. Yeager, D. Tryk, U. Landau, J. Wainright, D. Weng, K. Lux, M. Litt, C. Rogers, J. Electrochem. Soc. 141 (1994) L46–L48.
[81] R.W. Kopirzke, C.A. Linkous, G.L. Nelson, Polym. Degrad. Stab. 67 (2000) 335–344.
[82] G. Inzelt, M. Pineri, J.W. Schultze, M.A. Vorotyntsev, Electrochim. Acta 45 (2000) 2403–2421.
[83] G. Alberti, M. Casciola, Annu. Rev. Mater. Res. 33 (2003) 129–154.
[84] O. Savadogo, J. Power Sources 127 (2004) 135–161.
[85] J.A. Kerres, J. Membr. Sci. 185 (2001) 3–27.
[86] H. Wang, B.A. Holmberg, L. Huang, Z. Wang, A. Mitra, J.M. Norbeck, Y. Yan, J. Mater. Chem. 12 (2002) 834–837.
[87] P.L. Antonucci, A.S. Arico, P. Creti, E. Ramunni, V. Antonucci, Solid State Ionics 125 (1999) 431–437.
[88] Z.G. Shao, H. Xu, M. Li, I.-M. Hsing, Solid State Ionics 177 (2006) 779–785.
[89] Y. Song, J.M. Fenton, H.R. Kunz, L.J. Bonville, M.V. Williams, J. Electrochem. Soc. 152 (2005) A539–A544.
[90] K.T. Adjemian, S.J. Lee, S. Srinivasan, J. Benziger, A.B. Bocarly, J. Electrochem. Soc. 149 (2002) A256–A261.
[91] Y.M. Kim, S.H. Choi, H.C. Lee, M.Z. Hong, K. Kim, H.I. Lee, Electrochim. Acta 49 (2004) 4787–4796.
[92] P. Costamagna, C. Yang, A.B. Bocarsly, S. Srinivasan, Electrochim. Acta 47 (2002) 1023–1033.
[93] V. Ramani, H.R. Kunz, J.M. Fenton, J. Membr. Sci. 232 (2004) 31–34.
[94] V. Ramani, H.R. Kunz, J.M. Fenton, Electrochim. Acta 50 (2004) 1181–1187.
[95] S.H. Kwak, T.H. Yang, C.S. Kim, K.H. Yoon, Electrochim. Acta 50 (2004) 653–657.
[96] S.H. Kwak, T.H. Yang, C.S. Kim, K.H. Yoon, Solid State Ionics 160 (2003) 309–315.
[97] Y. Si, H.R. Kunz, J.M. Fenton, J. Electrochem. Soc. 151 (2004) 623–631.
[98] Y.F. Zhai, H.M. Zhang, J.W. Hu, B.L. Yi, J. Membr. Sci. (2006) in press.
[99] N. Shibuya, R.S. Porter, Macromolecules 25 (1992) 6495–6499.
[100] T. Kobayashi, M. Rikukawa, K. Sanui, N. Ogata, Solid State Ionics 106 (1998) 219–225.
[101] X. Guo, J. Fang, T. Watari, K. Tanaka, H. Kita, K.I. Okamoto, Macromolecules 35 (2002) 6707–6713.
[102] K. Ramya, B. Vishnupriya, K.S. Dhathathreyan, J. New Mater. Electrochem. Syst. 4 (2001) 115–120.
[103] J. Kerres, W. Cui, R. Disson, W. Neubrand, J. Membr. Sci. 139 (1998) 211–225.
[104] C. Hasiotis, V. Deimede, C. Kontoyannis, Electrochim. Acta 46 (2001) 2401–2406.
[105] A.D. Child, J.R. Reynolds, Macromolecules 27 (1994) 1975–1977.
[106] J.A. Asensio, S. Borros, P. Gomez-Romero, J. Membr. Sci. 241 (2004) 89–93.
[107] R.H. He, Q.F. Li, G. Xiao, N.J. Bjerrum, J. Membr. Sci. 226 (2004) 169–184.
[108] P. Staiti, M. Minutoli, S. Hocevar, J. Power Sources 90 (2000) 231–235.
[109] P. Staiti, M. Minutoli, J. Power Sources 94 (2001) 9–13.
[110] Q.F. Li, H.A. Hjuler, N.J. Bjerrum, J. Appl. Electrochem. 31 (2001) 773–779.
[111] J.T. Wang, R.F. Savinell, J.S. Wainright, M. Litt, H. Yu, Electrochim. Acta 41 (1996) 193–197.
[112] V. Deimede, G.A. Voyiatzis, J.K. Kallitsis, L. Qingfeng, N.J. Bjerrum, Macromolecules 33 (2000) 7609–7617.
[113] Q.F. Li, H.A. Hjuler, C. Hasiotis, J.K. Kallitsis, C.G. Kontoyanni, N.J. Bjerrum, Electrochem. Solid State Lett. 5 (2002) A125–A128.
[114] C. Hasiotis, L. Qingfeng, V. Deimede, J.K. Kallitsis, C.G. Kontoyannis, N.J. Bjerrum, J. Electrochem. Soc. 148 (2001) A513–A519.
[115] S.Y. Ahn, S.J. Shin, H.Y. Ha, S.A. Hong, Y.C. Lee, T.W. Lim, I.H. Oh, J. Power Sources 106 (2002) 295–303.
[116] DOE, R&D Plan for the High Temperature Membrane Working Group, 2002.
[117] B. Bauer, D.J. Jones, J. Roziere, L. Tchicaya, G. Alberti, M. Casciola, L. Massinelli, A. Peraio, S. Besse, E. Ramunni, J. New Mater. Electrochem. Syst. 3 (2000) 93–98.
[118] E. Endoth, S. Terazono, H. Widjaja, The Electrochemical Society Meeting Abstracts, vol. 2002-2, Salt Lake City, UT, October 20–24, 2002 (Abstract 89).
[119] S.R. Samms, S. Wasmus, R.F. Savinell, J. Electrochem. Soc. 143 (1996) 1498–1504.
[120] X. Glipa, M.E. Haddad, D.J. Jones, J. Rozie‘re, Solid State Ionics 97 (1997) 323–331.
[121] M. Rikukawa, K. Sanui, Prog. Polym. Sci. 25 (2000) 1463–1502.
[122] R.W. Lindstrom, US Patent 4,647,359 (1987).
[123] E.A. Ticianelli, C.R. Derouin, S. Sninivasan, J. Electroanal. Chem. 251 (1988) 275–295.
[124] H.A. Gasteiger, J.E. Panels, S.G. Yan, J. Power Sources 127 (2004) 162–171.
[125] H.A. Gasteiger, W. Gu, R. Makharia, M.F. Mathias, B. Sompalli, Beginning-of-life MEA performance–efficiency loss contributions, in: W. Vielstich, A. Lamm, H.A. Gasteiger (Eds.), Handbook of Fuel Cells: Fundamentals, Technology, and Applications, vol. 3, Wiley, 2003, pp. 593–609 (Chapter 46).
[126] Y. Song, Y. Wei, H. Xu, M. Williams, Y.X. Liu, L.J. Bonville, H.R. Kunz, J.M. Fenton, J. Power Sources 141 (2005) 250–257.
[127] L.J. Bonville, H.R. Kunz, Y. Song, A. Mientek, M. Williams, A. Ching, J.M. Fenton, J. Power Sources 144 (2005) 107–112.
[128] E. Higuchi, H. Uchida, T. Fujinami, M. Watanabe, Solid State Ionics 171 (2004) 45–49.
[129] O. Nishikawa, T. Sugimoto, S. Nomura, K. Doyama, K. Miyatake, H. Uchida, M. Watanabe, Electrochim. Acta 50 (2004) 667–672.
[130] http://www.c-na.de/media/apu/Referate/B02_Kundler.pdf, http://www.pemeas.com/images/gallery/highRes/celtecPPerformance.jpg.
[131] http://www.etek-inc.com/standard/index.php#MEA.
[132] http://www.agc.co.jp/english/news/2004/0928_e.pdf.
[133] A. Sun, Y.C. Chiu, F.B. Weng, Int. J. Energy Res. 29 (2005) 409–425.
[134] X. Li, I. Sabir, Int. J. Hydr. Energy 30 (2005) 359–371.
[135] C.A. Reiser, R.D. Sawyer, US Patent 4,769,297 (1988).
[136] C.A. Reiser, US Patent 4,826,742 (1989).
[137] A. Pollegri, P.M. Spaziante, US Patent 4,197,178 (1980).
[138] D.S. Watkins, K.W. Dircks, D.G. Epp, US Patent 4,988,583 (1991).
[139] D.P. Wilkinson, G.J. Lamont, H.H. Voss, C. Schwab, US Patent 5,521,018 (1996).
[140] D.S. Watkins, K.W. Dircks, D.G. Epp, US Patent 5,108,849 (1992).

[141] R.H. Marvin, C.M. Carlstrom, US Patent 6,500,580 (2002).
[142] M.W. Davis, Electronic Thesis, Mechanical Engineering Department, Virginia Tech., 2000.
[143] W.F. Michael, L. Alpred, Chem. Eng. Educat. 38 (2004) 236–240.
[144] V.A. Paganin, T.J.P. Freire, E.A. Ticinelli, E.R. Gonzalez, Rev. Sci. Instrum. 68 (1997) 3540–3543.
[145] Parker O-Ring Handbook, Section II, Basic O-Ring Elastomers, P2-11, Parker Hannifin Corporation, Cleveland, OH, 1999. http://www.parker.com/o-ring/Literature/ORD5700.pdf.
[146] K. Broka, P. Ekdunge, J. Appl. Electrochem. 27 (1997) 117–123.
[147] T. Sakai, H. Takenaka, E. Torikai, J. Electrochem. Soc. 133 (1986) 88–92.
[148] T. Sakai, H. Takenaka, N. Wakabayashi, Y. Kawami, E. Torikai, J. Electrochem. Soc. 132 (1985) 1328–1332.
[149] J. Fournier, G. Faubert, J.Y. Tilquin, R. Cote, D. Guay, J.P. Dodelet, J. Electrochem. Soc. 144 (1997) 145–154.
[150] T.R. Ralph, G.A. Hards, J.E. Keatins, S.A. Campbell, D.P. Wilkinson, M. Davis, J. St-Pierre, M.C. Johnson, J. Electrochem. Soc. 144 (1997) 3845–3857.
[151] M. Sluyters-Rehbach, Pure Appl. Chem. 66 (1994) 1831–1891.
[152] J. Benavente, M. Oleinikova, M. Munoz, M. Valiente, J. Electroanal. Chem. 451 (1998) 173–180.
[153] T.J.P. Freire, E.R. Gonzalez, J. Electroanal. Chem. 503 (2001) 57–68.
[154] J.M. Song, S.Y. Cha, W.M. Lee, J. Power Sources 94 (2001) 78–84.
[155] L. Giorgi, E. Antolini, A. Pozio, E. Passalacqua, Electrochim. Acta 43 (1998) 3675–3680.
[156] V.A. Paganin, C.L.F. Oliveira, E.A. Ticianelli, T.E. Springer, E.R. Gonzalez, Electrochim. Acta 43 (1998) 3761–3766.
[157] M. Ciureanu, R. Roderge, J. Phys. Chem. B 105 (2001) 3531–3539.
[158] J.-D. Kim, Y.-I. Park, K. Kobayashi, M. Nagai, M. Kunimatsu, Solid State Ionics 140 (2001) 313–325.